


RESEARCH ARTICLE



Transcription factor FOXM1 specifies chromatin DNA to extracellular vesicles

Yunsheng Zhang^{a,b}, Nana Ding^a, Yizhen Li^a, Min Ouyang^a, Ping Fu^a, Yousong Peng^a, and Yongjun Tan ^a

^aState Key Laboratory of Chemo/Biosensing and Chemometrics, College of Biology, Hunan Engineering Research Center for Anticancer Targeted Protein Pharmaceuticals, Hunan University, Changsha, Hunan, PR China; ^bThe Second Affiliated Hospital, University of South China, Hengyang, Hunan, PR China

ABSTRACT

Extracellular vesicle DNAs (evDNAs) hold significant diagnostic value for various diseases and facilitate transcellular transfer of genetic material. Our study identifies transcription factor FOXM1 as a mediator for directing chromatin genes or DNA fragments (termed FOXM1-chDNAs) to extracellular vesicles (EVs). FOXM1 binds to MAP1LC3/LC3 in the nucleus, and FOXM1-chDNAs, such as the *DUX4* gene and telomere DNA, are designated by FOXM1 binding and translocated to the cytoplasm before being released to EVs through the secretory autophagy during lysosome inhibition (SALI) process involving LC3. Disrupting FOXM1 expression or the SALI process impairs FOXM1-chDNAs incorporation into EVs. FOXM1-chDNAs can be transmitted to recipient cells via EVs and expressed in recipient cells when they carry functional genes. This finding provides an example of how chromatin DNA fragments are specified to EVs by transcription factor FOXM1, revealing its contribution to the formation of evDNAs from nuclear chromatin. It provides a basis for further exploration of the roles of evDNAs in biological processes, such as horizontal gene transfer.

Abbreviation: ATG5: autophagy related 5; CCFs: cytoplasmic chromatin fragments; ChIP: chromatin immunoprecipitation; cytoDNA: cytoplasmic DNA; CQ: chloroquine; FOXM1-DBD: FOXM1 DNA binding domain; *DUX4*: double homeobox 4; EVs: extracellular vesicles; evDNAs: extracellular vesicle DNAs; FOXM1: forkhead box M1; FOXM1-chDNAs: chromatin DNA fragments directed by FOXM1 to EVs; HGT: horizontal gene transfer; LC3-II: lipid modified LC3; LMNB1: lamin B1; LIR: LC3-interacting region; MAP1LC3/LC3: microtubule associated protein 1 light chain 3; MVBs: multivesicular bodies; M1-binding DNA: a linear DNA containing 72× FOXM1 binding sites; SALI: secretory autophagy during lysosome inhibition; siRNA: small interfering RNA; TetO-*DUX4*: TetO array-containing *DUX4* DNA; TetO: tet operator; TetR: tet repressor

ARTICLE HISTORY

Received 13 August 2023
Revised 31 October 2023
Accepted
10 November 2023

KEYWORDS

evDNAs; EVs; FOXM1;
FOXM1-chDNAs; LC3; SALI

Introduction

Extracellular vesicles (EVs) are membranous vesicles released by various cells into extracellular microenvironment and contain DNAs, RNAs, and proteins that serve as intercellular messengers for exchanging materials among cells [1,2]. Because extracellular vesicle DNAs (evDNAs) carry portions of genetic material from their parent cells under certain physiological or pathological conditions, extensive studies have focused on the diagnostic value of evDNAs for multiple diseases, while their biological functions are not explored as deeply as those of RNAs or proteins of EVs [3,4]. evDNAs have been suggested to play a role in so-called horizontal gene transfer (HGT) [5], which facilitates the exchange of functional genes and DNA fragments between cells [6]. Increasing evidence indicates that EVs contain functional genes or chromosome DNA fragments as evDNAs and transfer them to recipient cells [7]. For instance, LINE-1 retrotransposon as an evDNA is transferred horizontally among human cancer cells [8]. Another example is that telomere DNA carried by the EVs from antigen-presenting cells (APCs) is horizontally transferred to primarily naïve T cells and central memory T cells [9]. Therefore, understanding how chromatin DNA

fragments are selected to EVs is critical not only to advance the application of evDNAs in diagnosis, but also to clarify their functions in important biological processes such as HGT.

Recently, chromatin DNA has been found to translocate to the cytoplasm through the interaction between LMNB1 (lamin B1) and LC3 in the nucleus during autophagy [10], providing a clue to explore the origin of evDNAs. LC3 is a key member of the Atg8 family proteins responsible for autophagy cargo selection [11]. In addition to existing in the cytoplasm, LC3 is present in the nucleus and interacts with chromatin-binding LMNB1 (a nuclear lamina protein [12]). During macroautophagy/autophagy, a portion of regular LC3 (LC3-I) needs to be conjugated with phosphatidylethanolamine (PE) to form LC3-PE (LC3-II), which is called LC3 lipidation and allows LC3 protein to embed itself in membranes and then load cargos into autophagosomes [13]. Although autophagosomes are classically fused with lysosomal pathway for degradation [14], accumulated evidence shows that autophagosomes can secrete their components by releasing extracellular vesicles and particles [15]. Notably two major secretory autophagy pathways have been recently described: the LC3-

dependent EV loading and secretion (LDELS) that captures cargos at late endosomes [16] and the secretory autophagy during lysosome inhibition (SALI) that secrete cargos when degradation is impaired [17]. During SALI process, ATG14 (autophagy related 14) promotes the fusion of autophagosomes and endolysosomes to form multivesicular bodies (MVBs) that contain LC3-positive intraluminal vesicles (ILVs) [18]. ILVs can be released to extracellular environment as EVs through the fusion of MVBs with cell membrane [19]. It's well known that LC3 specifies the loading of proteins and RNAs to EVs [16,20]. However, because LMNB1 has no sequence specificity for its DNA binding [21], it is difficult to understand how certain chromatin DNA fragments are selected and loaded to EVs, if only based on the LMNB1-LC3-mediated mechanism of chromatin DNA cytoplasmic translocation.

Here, we show a transcription factor-LC3-involved mechanism that specifies certain chromatin genes or DNA fragments to EVs during autophagy. FOXM1, a member of forkhead box transcription factor family [22], participates in regulating cell proliferation [23], DNA damage repair [24], cell stemness [25], and metastasis [26,27] by stimulating gene transcription in nucleus [28]. FOXM1 can direct its chromatin binding regions directly through its DNA-binding consensus sequence [29] or indirectly by interacting with other transcription factors such as MYBL2/B-Myb, MuvB, and NFY [30]. In this study, we confirm that FOXM1 interacts with LC3 in nucleus and mediates the specific chromatin DNA fragments (termed FOXM1-chDNAs) to EVs during autophagy. The interaction between FOXM1 and LC3 is mediated by FOXM1's LC3-interacting region (LIR) motif (FOXM1 317-320aa) and facilitated by LC3 lipidation, while FOXM1-LC3 interaction does not disrupt FOXM1's DNA binding ability. FOXM1-chDNAs, including the DUX4 gene and telomere DNA, are identified by analyzing sequencing data from FOXM1-specific ChIP-seq, LC3-specific ChIP-seq, and evDNA-seq. The translocation of FOXM1-chDNAs to EVs is confirmed by DNA-FISH experiments, tracing the movement of selected chromatin loci with TetO-TetR-GFP method, and PCR analysis of DNA samples from MVBs and EVs. We confirm that FOXM1 expression and SALI process are essential for FOXM1-chDNAs to EVs. This study presents the first instance of directing chromatin DNA fragments in EVs by a transcription factor, providing a basis for further investigation of evDNAs' functions in biological processes, such as HGT functions in biological processes, such as HGT.

Results

The interaction between FOXM1 and LC3

Firstly, we identified LC3 as a potential partner interacting with transcription factor FOXM1, which directly or indirectly bound to the specific regions on chromatin, from our mass spectrometry analysis of the FOXM1 interactome, implicating that FOXM1 might participate in directing and loading chromatin DNA fragments to EVs. To test this hypothesis, we first confirmed the interaction between FOXM1 and LC3 in nucleus of lung cancer A549 cells. The

immunostaining of endogenous FOXM1 and LC3 showed that the two proteins were colocalized in the nucleus with the Pearson's Correlation Coefficient value around 0.66 ± 0.08 (Figure 1A). The co-immunoprecipitation (co-IP) experiments revealed that FOXM1 interacted with LC3, particularly with lipidated LC3-II in nucleus (Figure 1B and Figure S1A-B). A bimolecular fluorescence complementation (BiFC) assay [31] further confirmed that FOXM1-LC3 interaction occurred primarily in nucleus (Figure 1C). The co-IP of exogenous Flag-FOXM1 with WT GFP-LC3 or GFP-LC3^{G120A} mutant, which disrupted LC3 lipidation on its G120 residue [10], showed that LC3 lipidation deficiency decreased FOXM1-LC3 interaction (Figure S1C-D), suggesting that LC3 embedding in nuclear membranes facilitated its interaction with FOXM1.

Next, we identified FOXM1 and LC3 regions to mediate FOXM1-LC3 interaction. We screened the FOXM1 protein and found that the FOXM1 DNA-binding domain (FOXM1-DBD) was required for its LC3 binding (Figure 1D) and FOXM1-DBD interacted with LC3 in GST-LC3-affinity-isolation assays (Figure 1E). In addition, overexpression of GFP-FOXM1-DBD abolished endogenous FOXM1-LC3 interaction (Figure S1E-F). It was known that so-called LIR motif existed in LC3' substrate proteins [32,33]. We screened the FOXM1-DBD sequence and identified four LIR motifs (263–266, 273–276, 307–310 and 317–320), which were evolutionarily conserved among FOXM1s from human, mouse, rat, and macaque (Figure S1G). We generated four FOXM1-DBD mutants (Y263A, F273A, F307A, and Y317A, corresponding to the four LIR motifs respectively), of which only the Y317A mutation on FOXM1-DBD abolished its interaction with LC3 in GST-LC3-affinity-isolation assays (Figure 1F), suggesting that the LIR motif (317–320) in FOXM1-DBD mediated FOXM1-LC3 binding. On the other hand, because LC3 residues R10, R11, and F52 mediated LC3 binding to its protein partners [10,34], we tested whether the LC3 aa1–28 region (containing R10 and R11) or LC3 aa29–128 region (containing F52) could interact with FOXM1 in GST-affinity-isolation assays. We found that only the aa29–128 region (containing F52) of LC3 interacted with FOXM1 (Figure 1G), suggesting that LC3 F52 residues mediated LC3- FOXM1 binding. Thus, we generated an LC3 aa29–128 truncated F52A mutant and found that this mutant could not bind to FOXM1 in GST-affinity-isolation assays (Figure 1H). Rosetta Dock [35] was performed with the known structures of FOXM1-DBD [36] and LC3 [37] to simulate FOXM1-LC3 interaction and predicted the formation of hydrogen bonds between FOXM1's LIR motif (317–320) and LC3's F52 residue (Figure 1I), further supporting the conclusion of FOXM1-LC3 interaction in biochemical experiments.

To test whether LC3 binding to FOXM1-DBD affected FOXM1's DNA binding ability, we performed the electrophoretic mobility shift assays (EMSAs) with recombinant FOXM1 proteins and a FAM-labeled DNA probe containing putative FOXM1 binding sites. We observed that the DNA probe formed FOXM1-DNA complexes with FOXM1 alone, and created a supershift of LC3-FOXM1-DNA complexes by adding recombinant LC3 proteins in the reactions (Figure 1J),

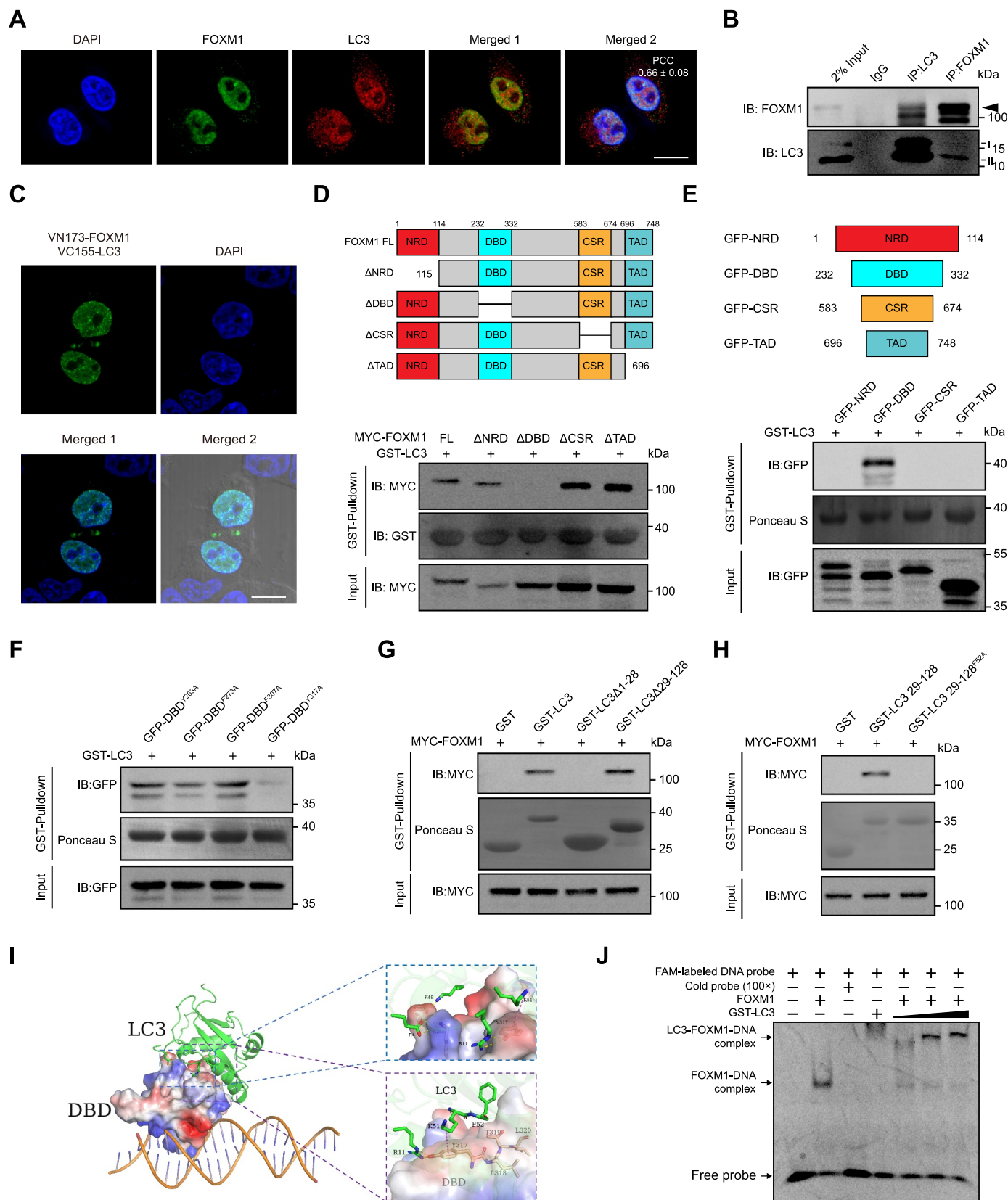


Figure 1. The interaction between FOXM1 and LC3. (A) Representative FOXM1 and LC3 images in A549 cells that were fixed by 4% paraformaldehyde and immunostained with anti-FOXM1 and anti-LC3 antibodies. Scale bar: 10 μ m. The Pearson correlation coefficient (PCC) value of FOXM1 and LC3 colocalization was 0.66 ± 0.08 . (B) Co-immunoprecipitation of endogenous FOXM1 and LC3 in A549 cells. (C) The BiFC assays of FOXM1-LC3 interaction. HEK293T cells were transfected with the indicated combination of split Venus constructs for 24 h. Scale bar: 10 μ m. (D) HEK293T cells (5×10^6) were transfected with MYC-tagged FOXM1 deletion mutant plasmids (5 μ g). All cell lysates were affinity isolated with bacterially purified GST-LC3 protein (30 μ g) and subjected to immunoblotting as indicated. (E) The GFP-fused FOXM1 truncations were expressed and affinity isolated with bacterially purified GST-LC3 as described above. (F) The GFP-fused FOXM1-DBD point mutations were expressed and affinity isolated with bacterially purified GST-LC3 as described above. (G) The MYC-tagged FOXM1 was affinity isolated with bacterially purified GST-LC3 truncated mutants as described above. (H) The MYC-tagged FOXM1 was expressed and affinity isolated with bacterially purified GST-LC3 truncated point mutants as described above. (I) The molecular docking simulation for FOXM1-LC3 interaction by Rosetta Dock. (J) EMSA showed FOXM1, LC3 and DNA formed LC3-FOXM1-DNA complex.

suggesting that the FOXM1-LC3 interaction did not impair FOXM1's DNA binding ability and that the LC3-FOXM1-DNA complex could be formed in cells.

FOXM1-chDNAs were specified to extracellular vesicles during autophagy

LC3 and FOXM1 immuno-staining and DNA DAPI-staining of A549 cells showed that DNAs, FOXM1, and LC3 colocalized in cytoplasmic vesicles (Figure 2A and Figure S2A), whose numbers were increased (from 3% in control cells to 15% in starvation-treated cells) (Figure 2B) by starvation-induced autophagy, which was confirmed by the increased formation of LC3-positive autophagosomes (Figure S2B), the elevated levels of autophagy marker LC3-II and the decreased levels of autophagy cargo receptor SQSTM1/p62 (sequestome 1) [38] in the cells (Figure S2C). Similar phenomena were also observed from multiple human cell lines, such as HeLa and HEK293T cells, or cells treated with different autophagy-inducing conditions, such as treatment with no amino acid or rapamycin (20 μ M) (Figure S2D). The BiFC assays with exogenous VN173-FOXM1 and VC155-LC3 further confirmed that FOXM1 and LC3 co-existed in cytoplasmic DNA-containing vesicles (Figure 2C). Interestingly, the expression of RFP-FOXM1 Δ DBD, in which FOXM1-DBD was deleted, could not appear in cytoplasmic DNA-containing vesicles (Figure S2E), confirming that the FOXM1 DNA-binding ability was required for the formation of cytoplasmic LC3-FOXM1-DNA vesicles during autophagy. It is acknowledged that heterochromatin fragments are released from the nucleus and form cytoplasmic chromatin fragments (CCFs) in senescent cells [10,39] and CCFs activate CGAS-STING1 pathway in the cytoplasm [40]. In order to differentiate between LC3-FOXM1-DNAs and CCFs, a series of experiments were conducted. GLB1/ β -galactosidase staining was performed to demonstrate that starvation did not induce cellular senescence in A549 cells (Figure S2F). Immunofluorescent staining revealed the absence of γ -H2AX foci and weak signals of CCF marker H3K9me3 in cytoplasmic LC3-FOXM1-chDNAs vesicles in starved A549 cells (Figure S2G-H). Furthermore, western blotting demonstrated that neither the protein levels of DNA damage marker γ -H2AX, nor the cytoplasmic DNA sensor STING1 or p-STING1, were induced in starved-A549 cells (Figure S2I). Collectively, these findings suggested that cellular senescence, DNA damage, or the CGAS-STING1 pathway were not major events in the context of starvation in the cells, so that the formation of cytoplasmic LC3-FOXM1-DNAs was independent of CCF mechanisms.

Next, we collected EVs (including Large EVs (LEVs) and Small EVs (sEVs)) from starved A549 cells by serial differential ultracentrifugation [41] (Figure S3A). We showed that both FOXM1 and LC3 were present in EV samples by western blotting, same as histone 3 (Figure 2D). Because researchers typically focused on sEVs when studying EVs [42,43] and only the sEVs from our samples possessed the TSG101 EV marker [44] (Figure 2D), we just collected sEVs as EV samples in subsequent experiments and characterized their size range around 80–250 nm through nanoparticle tracking analysis and transmission electron microscopy (Figure S3B-C). DNA

samples from EVs (evDNAs) were purified and analyzed by vertical agarose gel electrophoresis (Figure 2E), which showed evDNAs in the range of 2 to 15 kb (mostly around 12 kb), confirming that DNA, FOXM1, and LC3 co-existed in EV samples.

To identify the chromatin DNA fragments specified by FOXM1 (FOXM1-chDNAs) that finally existed in EVs, we first performed chromatin immunoprecipitation sequencing (ChIP-seq) analysis for FOXM1 or LC3 separately with starved A549 cells and obtained 103 specific loci on chromatin bound by both FOXM1 and LC3 (Table S1) from overlapping FOXM1-ChIP fragments (GSE216672) and LC3-ChIP fragments (GSE216672). We then performed evDNA-sequencing analysis with EVs of starved A549 cells and obtained the fragments of evDNAs (GSE216672). After analyzing the overlapped sequences of FOXM1-LC3 ChIP loci and evDNAs, we identified 25 chromatin loci as FOXM1-chDNAs (Table 1), which could be annotated as functional genes ($n=8$, including the *DUX4* gene), telomere ($n=1$), centromere ($n=8$), and nonsense regions ($n=8$). We selected three FOXM1-chDNAs (FOXM1-chDNA1 from a telomere locus, FOXM1-chDNA2 from a nonsense region, and FOXM1-chDNA3 from *DUX4* locus) as examples to perform ChIP-qPCR and confirmed FOXM1 and LC3 binding to these FOXM1-chDNAs at chromatin but not to the control region such as the *ACTB*/ β -actin promoter (Figure S3D-E).

To verify that FOXM1-chDNAs were translocated to the cytoplasm and finally existed in EVs, we first purified cytoplasmic DNA (cytoDNA) particularly [45] and found that the levels of the three FOXM1-chDNAs were elevated in the cytoplasm of starved A549 cells (Figure 2F). A DNA-FISH probe (10 Kb) specific to the FOXM1-chDNA1-adjacent region was generated and DNA-FISH experiments showed that FOXM1-chDNA1 appeared in the cytoplasm post starvation (Figure 2G), confirming that FOXM1-chDNAs were translocated to the cytoplasm during

Table 1. The list of FOXM1-chDNAs identified from the EVs during autophagy.

Names	Sequence signatures	Chr	genelD
FOXM1-chDNA1	Telomere	18	ENSG00000263006
FOXM1-chDNA2	Nonsense region	9	ENSG00000228522
FOXM1-chDNA3	Coding region (<i>DUX4</i>)	4	ENSG00000260596
FOXM1-chDNA4	Coding region (<i>PGK1</i>)	X	ENSG00000102144
FOXM1-chDNA5	Coding region (<i>ITFG2</i>)	12	ENSG00000111203
FOXM1-chDNA6	Coding region (<i>FOXM1</i>)	12	ENSG00000111206
FOXM1-chDNA7	Coding region (<i>FOXM1</i>)	12	ENSG00000111206
FOXM1-chDNA8	Coding region (<i>TBC1D5</i>)	3	ENSG00000131374
FOXM1-chDNA9	Coding region (<i>XR_946063.2</i>)	10	ENSG00000166317
FOXM1-chDNA10	Coding region (<i>XR_943570.1</i>)	14	ENSG00000258314
FOXM1-chDNA11	Centromere	5	ENSG00000170571
FOXM1-chDNA12	Centromere	1	ENSG00000224857
FOXM1-chDNA13	Centromere	20	ENSG00000227195
FOXM1-chDNA14	Centromere	3	ENSG00000251727
FOXM1-chDNA15	Nonsense region	16	ENSG00000261239
FOXM1-chDNA16	Nonsense region	16	ENSG00000261239
FOXM1-chDNA17	Nonsense region	16	ENSG00000261239
FOXM1-chDNA18	Nonsense region	16	ENSG00000261239
FOXM1-chDNA19	Nonsense region	16	ENSG00000261239
FOXM1-chDNA20	Centromere	17	ENSG00000263433
FOXM1-chDNA21	Centromere	17	ENSG00000263433
FOXM1-chDNA22	Centromere	17	ENSG00000263433
FOXM1-chDNA23	Centromere	17	ENSG00000264970
FOXM1-chDNA24	Nonsense region	1	ENSG00000276118
FOXM1-chDNA25	Nonsense region	5	ENSG00000284042

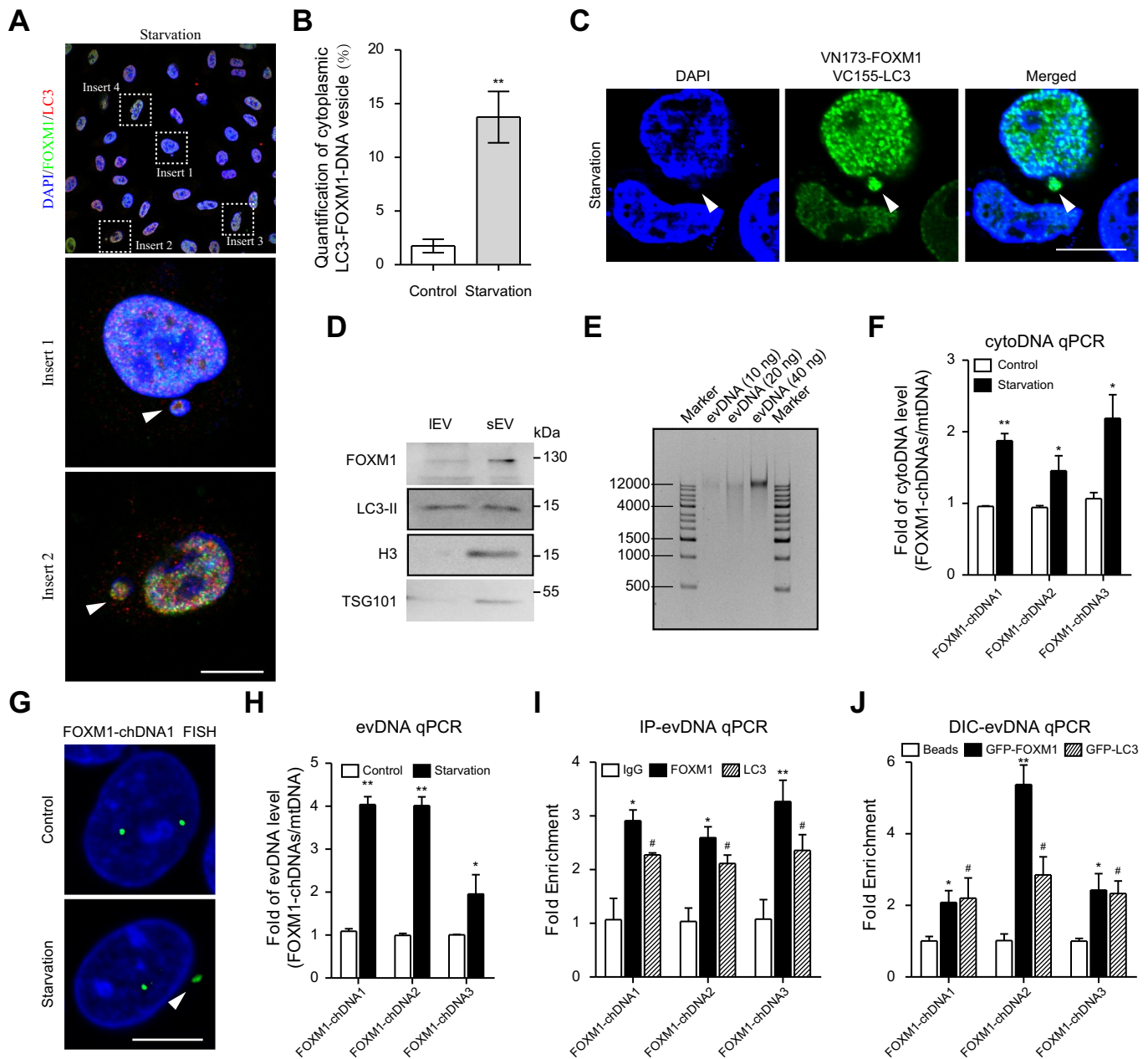


Figure 2. FOXM1-chDNAs were specified to extracellular vesicles during autophagy. (A) Representative LC3-FOXM1-DNA vesicles image in the cytoplasm of starved A549 cells (6 h) that were immunostained with anti-FOXM1 and anti-LC3 antibodies. The white arrows indicated LC3-FOXM1-DNA vesicle. Scale bar: 10 μ m. (B) quantification of cytoplasmic LC3-FOXM1-DNA vesicle in non-starved or starved A549 cells (6 h). ($n = 4$ independent experiments). (C) the BiFC assays showed that the exogenous VN173-FOXM1, VC155-LC3 and chromatin DNA vesiculated in the cytoplasm of starved A549 cells (6 h). Scale bar: 10 μ m. (D) EVs were collected from starved A549 cells (48 h) and subjected to immunoblotting for TSG101, H3, FOXM1 and LC3. (E) evDNAs were purified from EVs collected from starved A549 cells (48 h). The different concentrations of evDNAs were analyzed by 1% vertical agarose gel electrophoresis. (F) the cytoplasmic DNA (cytoDNA) was extracted from non-starved or starved A549 cells (24 h) for qPCR. The mitochondria DNA (mtDNA, *ND-2* gene) was used as the internal loading control. (G) Representative DNA-FISH images of FOXM1-chDNA1-adjacent region (10 Kb probe) in starved A549 cells (6 h). The white arrows indicated FOXM1-chDNA1. (H) the evDNA was extracted from non-starved or starved A549 cells (48 h) for qPCR. The data were normalized by mtDNA. (I) the qPCR analyses of FOXM1-chDNAs in anti-FOXM1-IP evDNA or anti-LC3-IP evDNA from EVs collected from starved A549 cells (48 h). (J) the qPCR analyses of FOXM1-chDNAs in the DIC-purified GFP-FOXM1-specific EVs or DIC-purified GFP-LC3-specific EVs collected from starved A549 stably expressing GFP-FOXM1 or GFP-LC3 cells (48 h). Data information: in (B, F and J), data are presented as mean \pm SEM. * $P < 0.05$, # $P < 0.05$, ** $P < 0.01$; unpaired two-tailed.

autophagy. Then, we purified evDNAs from the EVs of starved A549 cells and found that the levels of the three FOXM1-chDNAs were elevated in EVs (Figure 2H), confirming that FOXM1-chDNAs were finally translocated to EVs during autophagy. The levels of the three FOXM1-chDNAs were also observed to be elevated in EVs obtained

from HeLa cells subjected to starvation or A549 cells treated with rapamycin (Figure S3F-G), suggesting that the chromatin DNA fragments specified by FOXM1 to EVs remained consistent across different cell types or different conditions of autophagy induction. In addition, we treated EVs of starved A549 cells with Plasmid-Safe ATP-

dependent DNase (PS), which only digested linear DNA [46], and observed the decreased levels of the three FOXM1-chDNAs from PS-treated samples (Figure S3H), identifying FOXM1-chDNAs as linear DNA outside the lumen of EVs. This result was consistent with the previous finding that evDNAs are mainly localized outside the lumen of EVs [47]. We also performed protease protection assays with EVs of starved A549 cells and observed the decreased levels of FOXM1 and LC3-II, but not HSPA/HSP70 [48] (Figure S3I), suggesting that FOXM1 and LC3-II residing on the outer surface of EVs. Then, we treated EVs of starved A549 cells with formaldehyde to cross-link their DNA and proteins, and EV lysates were immunoprecipitated with anti-FOXM1 or anti-LC3 antibodies for evDNA purification. The levels of the three FOXM1-chDNAs in FOXM1 or LC3 specific IP-evDNA samples were significantly elevated (Figure 2I), further confirming that FOXM1-chDNAs were bound by FOXM1 or LC3 on EVs. We also collected FOXM1-specific EVs or LC3-specific EVs with GFP-Trap from GFP-FOXM1 or GFP-LC3-overexpressing A549 cells via direct immunoaffinity capture (DIC) approach [1] and observed elevated levels of the three FOXM1-chDNAs in DIC samples (Figure 2J), suggesting that both exogenous GFP-FOXM1 and GFP-LC3 facilitated FOXM1-chDNAs to EVs. Together, this data suggested that FOXM1 and LC3 mediated FOXM1-chDNAs to EVs during autophagy.

FOXM1-chDNAs knocked-in with TetO array were specified to EVs

To confirm FOXM1-chDNAs translocation to EVs, we knocked in TetO array (96×) at the loci of selected FOXM1-chDNAs by CRISPR-cas9 in A549 cells (Figure S4A). DNAs containing TetO array were then visualized directly by exogenously expressing TetR-EGFP in cells [49]. Because telomere DNA was transferred to EVs [9], we first edited the adjacent FOXM1-chDNA1 region (a telomere locus) at chromosome 18 (Figure S4B) and observed TetO-telomere signals in nucleus followed by elevated levels in the cytoplasm post starvation (Figure S4C-D), confirming the validity of the TetO-TetR-GFP method. Next, we edited the FOXM1-chDNA3 locus (*DUX4* locus) at chromosome 4 (Figure S4B) for subsequent experiments. *DUX4* has been identified as a transcription factor that plays a role in embryonic development [50] and in promoting immune evasion of cancers [51]. The signals of TetO array-containing *DUX4* DNA (TetO-*DUX4*) could be visualized in nucleus of A549^{TetO-*DUX4*} cells and its cytoplasmic signals were induced by starvation (Figure 3A), which were further confirmed by qPCR analysis of TetO-*DUX4* in cytoDNA (Figure 3B). The TetO-*DUX4* signals observed in the cytoplasm after starvation were colocalized with the LC3 immunofluorescent signals (Figure 3C), confirming that FOXM1-chDNA3 (*DUX4* locus) appeared in autophagosomes during autophagy.

Next, we intended to test whether cytoplasmic TetO-*DUX4* appeared in MVBs. We used the discontinuous sucrose gradient method to prepare different fractions to define MVB compartments [52] from postnuclear supernatants of

A549^{TetO-*DUX4*} cells. Based on specific MVB markers, such as RAB7 [53], CD63 [54], or TSG101 [55], we first confirmed that FOXM1, like LC3, existed in MVB fractions (Figure 3D). DNA samples were prepared from harvested fractions and qPCR results specific to TetO-*DUX4* DNA showed significant enrichment in MVB fractions (Figure 3E). Furthermore, TetO-*DUX4* signaling in the cytoplasm after starvation was observed in certain CD63-positive regions (Figure 3F). We also isolated samples of MVBs by immunoprecipitating A549^{TetO-*DUX4*} cell lysates with anti-CD63 antibodies [56] to prepare their DNA, which showed elevated TetO-*DUX4* DNA levels in these MVBs compared to IgG-IP controls (Figure 3G), suggesting that this FOXM1-chDNA was transported to MVBs during autophagy.

We collected EVs from A549 cells and A549^{TetO-*DUX4*} cells to prepare DNA samples and PCR results confirmed that TetO-*DUX4* DNA appeared in EVs (Figure 3H). The starvation in A549^{TetO-*DUX4*} cells resulted in elevated levels of TetO-*DUX4* DNA in EVs (Figure 3I). We also collected EVs from A549^{TetO-*DUX4*} cells using the DIC approach with anti-FOXM1 or anti-LC3 antibodies to prepare DNA samples and observed elevated TetO-*DUX4* DNA levels in samples of FOXM1-specific EVs or LC3-specific EVs (Figure 3J), suggesting that FOXM1 and LC3 were involved in transferring TetO-*DUX4* DNA to EVs. Moreover, after EVs were treated with PS DNase, decreased levels of TetO-*DUX4* DNA were observed but not for mitochondrial DNA controls (Figure 3K), implicating TetO-*DUX4* DNA as linear DNA on EVs' outer membrane. Together, we confirmed that this FOXM1-chDNA was specified to EVs during autophagy.

FOXM1-chDNAs to EVs were relied on FOXM1 and SALL1 process

We found that PCR-amplified DNA samples from *DUX4* locus were able to affinity-isolate FOXM1 or lipidated LC3-II *in vitro* (Figure 4A), proving the two proteins bound to this FOXM1-chDNA. To confirm FOXM1's role in FOXM1-chDNAs to EVs, we generated an A549^{FOXM1-/-} cell line using CRISPR-cas9 technology targeting *FOXM1* gene in A549 cells (Figure S5A). In A549^{FOXM1-/-} cells, the levels of all three tested FOXM1-chDNAs (FOXM1-chDNA1 from a telomere locus, FOXM1-chDNA2 from a nonsense region, and FOXM1-chDNA3 from *DUX4* locus) were decreased in cytoplasm compared to wild type control cells post starvation in qPCR analysis of purified cytoDNA samples (Figure 4B). Consequently, EVs from A549^{FOXM1-/-} cells contained significantly lower levels of the three FOXM1-chDNAs than control cells post starvation (Figure 4C). Furthermore, we knocked down the expression of FOXM1 in A549^{TetO-*DUX4*} cells by *FOXM1* siRNA (Figure S5B) and observed that cytoplasmic levels of TetO-*DUX4* signaling were decreased in the cells post starvation (Figure 4D). In addition, we constructed a linear DNA containing 72× FOXM1 binding sites (M1-binding DNA) that was bound by recombinant FOXM1 *in vitro* (Figure S5C) or FOXM1-DBD-GFP protein *in vivo* when transfected into cells (Figure S5D). We transfected M1-binding DNA or control DNA in equal amounts into cells and qPCR analysis of isolated evDNA samples showed that

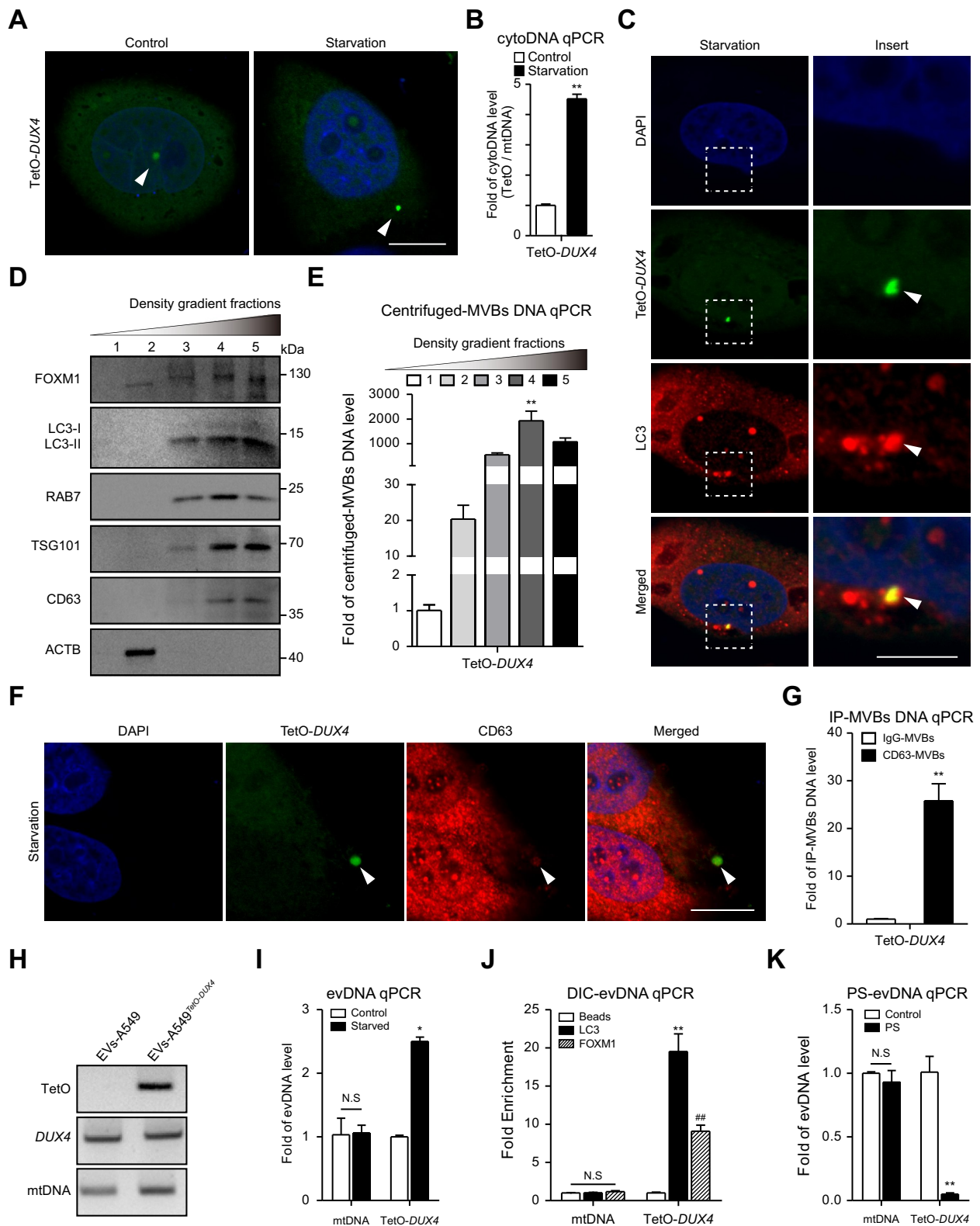


Figure 3. FOXM1-chDnas knocked-in with the TetO array were specified to EVs. (A) Representative TetO-DUX4 images in starved A549^{TetO-DUX4} cells (6 h) that were transiently expressed TetR-EGFP. The white arrows indicated TetO-DUX4. Scale bar: 10 μ m. (B) The A549^{TetO-DUX4} cells were treated with starvation and cytoplasmic DNA (cytoDNA) was extracted 24 h later for qPCR. The mtDNA was internal control. (C) Immunostaining of the endogenous LC3 and TetO-DUX4 in starved A549^{TetO-DUX4} cells (6 h) that were exogenously expressed TetR-EGFP. The white arrows indicated TetO-DUX4 that was translocated into cytoplasmic autophagosome. Scale bar: 10 μ m. (D) MVB compartments were isolated from starved A549^{TetO-DUX4} cells (24 h) by discontinuous sucrose gradient and subjected to immunoblotting. (E) The qPCR analyses of TetO-DUX4 in MVB fractions collected from starved A549^{TetO-DUX4} cells (24 h) by discontinuous sucrose gradient. (F) Immunostaining of the endogenous CD63 and TetO-DUX4 in starved-A549^{TetO-DUX4} cells (6 h). The white arrows indicated TetO-DUX4 that was translocated into cytoplasmic MVB. Scale bar: 10 μ m. (G) The qPCR analyses of TetO-DUX4 in MVBs collected from starved-A549^{TetO-DUX4} cells (24 h) by CD63-immunoprecipitation. (H) PCR was used to amplify the TetO-DUX4, DUX4, and mitochondria DNAs in the evDnas collected from starved A549^{TetO-DUX4} or A549^{TetO-DUX4} cells (48 h). (I) The qPCR analyses of TetO-DUX4 in the EVs collected from starved-A549^{TetO-DUX4} cells (48 h). (J) The qPCR analyses of TetO-DUX4 in the DIC-purified FOXM1-specific EVs or LC3-specific EVs collected from starved-A549^{TetO-DUX4} cells (48 h). (K) The qPCR analyses of TetO-DUX4 in the Plasmid-Safe ATP-dependent DNase (PS)-digested EVs collected from starved-A549^{TetO-DUX4} cells. Data information: in (B, E, G and K), data are presented as mean \pm SEM. * P < 0.05, # P < 0.05, ## P < 0.01, *** P < 0.01; unpaired two-tailed.

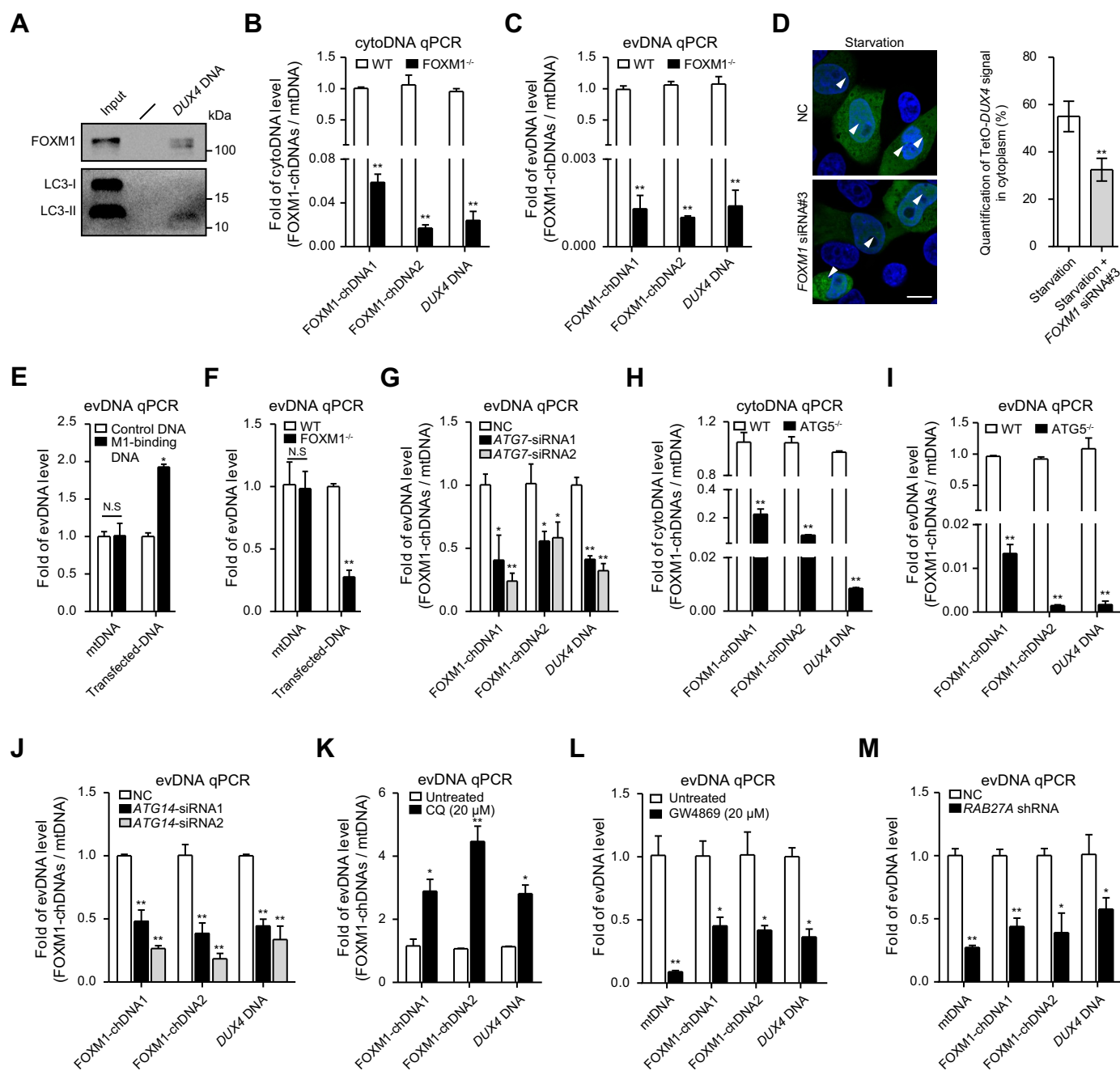


Figure 4. FOXM1-chDNAs to EVs were relied on FOXM1 and SALL1 process. (A) A549 cell lysates were incubated with biotinylated *DUX4* DNA (500 ng). The bound proteins were immunoprecipitated with streptavidin microbeads and blotted by anti-FOXM1 or LC3 antibodies. (B and C) the qPCR analyses of three FOXM1-chDNAs in the cytoplasm or EVs collected from starved A549 or A549^{FOXM1^{-/-}} cells. The data were normalized by mtDNA. (D) A549^{TetO-DUX4} cells were transfected with 50 nM *FOXM1* siRNA and 1 μg TetR-EGFP plasmid. After the transfection (48 h), cells were starved (6 h) and imaged for the signal of TetO-*DUX4* (left). The white arrows indicated TetO-*DUX4*. Scale bar: 10 μm. The TetO-*DUX4* signal in the cytoplasm was quantitated (right). (E) HEK293T cells were transfected with linear M1-binding or control DNA at the equal amount. After the transfection (24 h), all cells were starved (48 h) for collecting EVs. The qPCR analyses were performed for the mtDNA and transfected DNA in evDNAs purified from the EVs. (F) A549 and A549^{FOXM1^{-/-}} cells were transfected with linear M1-binding DNA at the equal amount. After the transfection (24 h), all cells were starved (48 h) for collecting EVs. The qPCR analyses were performed for the mtDNA and transfected DNA in evDNAs purified from the EVs. (G) the evDNAs were isolated from starved-A549 cells (24 h) that were transfected with ATG7 siRNA (48 h). The qPCR analyses of three FOXM1-chDNAs in these evDNAs. (H and I) the qPCR analyses of three FOXM1-chDNAs in the cytoplasm or EVs collected from starved A549 or A549^{ATG5^{-/-}} cells. The data were normalized by mtDNA. (J) the evDNAs were isolated from starved-A549 cells (24 h) that were transfected with ATG14 siRNA (48 h). The qPCR analyses of three FOXM1-chDNAs in these evDNAs. (K) EVs were collected from A549 cells that were treated with CQ (20 μM) and starvation (24 h). The qPCR analyses were performed for the three FOXM1-chDNAs in evDNAs purified from the EVs. (L) EVs were collected from A549 cells that were treated with GW4869 (20 μM) and starvation (24 h). The qPCR analyses were performed for the three FOXM1-chDNAs in evDNAs purified from the EVs. (M) EVs were collected from starved-A549 cells (24 h) that were infected by RAB27A shRNA lentiviruses. The qPCR analyses were performed for the three FOXM1-chDNAs in evDNAs purified from the EVs. Data information: in (B-M), data are presented as mean ± SEM. **P* < 0.05, ***P* < 0.01; unpaired two-tailed.

M1-binding DNA levels in EVs were higher than control DNA (Figure 4E), suggesting that FOXM1 facilitated FOXM1-recognized DNA fragments being transported to EVs. We also transfected M1-binding DNA into A549^{FOXM1-/-} cells and found that M1-binding DNA levels in EVs of A549^{FOXM1-/-} cells were significantly lower than those of wild-type control cells (Figure 4F). Together, the data suggested that FOXM1-chDNAs to EVs relied on FOXM1 in cells.

To confirm the formation of autophagosomes contributing FOXM1-chDNAs to EVs, we knocked down ATG7 (autophagy related 7), which facilitates LC3 lipidation and translocation to the phagophore membrane, the precursor of autophagosomes [57], in starved-A549 cells (Figure S5E) and identified an impaired transferring of FOXM1-chDNAs to EVs (Figure 4G). We also generated an A549^{ATG5-/-} cell line using CRISPR-cas9 technology targeting *ATG5* gene in A549 cells (Figure S5F). *ATG5* mediates LC3-dependent expansion of the phagophore membrane [58]. In A549^{ATG5-/-} cells, the cytoplasmic and EVs' levels of FOXM1-chDNAs were lower than that of control cells post starvation (Figure 4H-I), correlated with the decreased levels of FOXM1 and LC3 in the EVs from A549^{ATG5-/-} cells (Figure S5G). In addition, we knocked down ATG14, which promotes membrane tethering and fusion of autophagosomes to endolysosomes [18], in starved-A549 cells (Figure S5H) and found that the knockdown of ATG14 disrupted FOXM1-chDNAs transferring to EVs (Figure 4J), supporting that cytoplasmic LC3-FOXM1-DNA vesicles fused with endolysosomes via SALI process. The autophagy cargo receptor SQSTM1 [17] was detected in EVs (Figure S5I) provided additional support that SALI process facilitated the secretion of FOXM1-chDNAs.

To confirm the formation of MVBs that contribute FOXM1-chDNAs loading to EVs, A549 cells were treated with chloroquine (CQ), a lysosome inhibitor that facilitates MVB formation by inhibiting MVB-lysosome fusion [59,60]. We observed that the levels of FOXM1-chDNAs were elevated in EVs of the CQ-treated cells post starvation (Figure 4K). In addition, A549 cells were treated with a chemical compound GW4869, a neutral sphingomyelinase inhibitor that prevents intraluminal budding from the limiting membrane of the MVBs [61]. We collected EVs from equal numbers of A549 cells untreated or treated with GW4869 and found that the secretion of FOXM1, LC3 and TSG101 via EVs was decreased by GW4869 treatment (Figure S5J). By qPCR analysis of prepared evDNA samples, we observed that levels of the three FOXM1-chDNAs in EVs, similar to mtDNA, were decreased by GW4869 treatment, suggesting that FOXM1-chDNAs secretion to EVs was predominantly mediated by MVBs (Figure 4L). Furthermore, we knocked down RAB27A (member RAS oncogene family), which mediates fusion events between MVBs and the plasma membrane [62], in starved-A549 cells (Figure S5K) and found that the knockdown of RAB27A disrupted FOXM1-chDNAs transferring to EVs (Figure 4M). Together, the data suggested that EV-associated secretion of FOXM1-chDNAs were depended on MVB-involved SALI process.

Transfer of FOXM1-chDNAs to recipient cells via EVs

We verified that DiI-labeled EVs could be transferred intracellularly to A549 recipient cells (Figure S6A-B). We then incubated DIC-collected GFP-FOXM1⁺-EVs with cells and identified immune signals of GFP-FOXM1 in recipient cells (Figure 5A), correlated with stimulation of transcription of FOXM1 target genes, including *CDK1*, *PLK1*, and *CDC25B*, when compared to control EVs-treated cells (Figure S6C). Notably, we observed that DAPI-stained DNA signals colocalized with GFP-FOXM1 signals in the cytoplasm of recipient cells (Figure 5B), indicating that FOXM1-chDNAs were transmitted simultaneously to cells. Therefore, we used insect *Spodoptera frugiperda* SF-9 cells as recipient cells to absorb EVs from human cells because human evDNAs are distinct from insect genomic DNAs (Figure 5C). SF-9 cells were incubated with EVs from A549^{TetO-DUX4} cells and PCR analysis of extracted genomic DNA samples confirmed that TetO-DUX4 DNA was transmitted to SF-9 cells (Figure 5D). Long-term culture of SF-9 cells treated with EVs showed that TetO-DUX4 DNA was detectable even at week 4 post EV treatment in PCR-amplified genomic DNA samples (Figure 5E). In addition, we tracked TetO-DUX4 DNA from EVs in A549 recipient cells expressing TetR-EGFP and observed that TetO-DUX4 DNA entered recipient cells (Figure 5F). We also amplified FOXM1-chDNA3 from a modified *DUX4* locus, whose last exon was fused with GFP cDNA before the stop codon, and transfected the DNA into A549 cells. FOXM1-chDNA3 transfection alone resulted in the expression of DUX4-GFP protein in recipient cells (Figure 5G). Based on the fact that *DUX4* re-expression promotes cancer immune evasion [51], FOXM1-chDNA3 from EVs may have the potential to enhance the immune evasion phenotype of recipient cells. Overall, the data indicated that FOXM1-chDNAs were transferred to recipient cells via EVs and expressed in recipient cells when they carried functional genes.

Discussion

In our study, we have identified that the FOXM1 transcription factor is responsible for the packaging of chromatin DNA fragments into EVs. Specifically, FOXM1-chDNAs form LC3-FOXM1-DNA vesicles in the cytoplasm with FOXM1 and LC3 during autophagy. These cytoplasmic LC3-FOXM1-DNAs are released into EVs, which highlights the significance of transcription factors in determining EV derived DNA from chromatin DNA sources (as shown in Figure 6). FOXM1 can potentially identify specific chromatin binding regions, thus offering a strategy to identify EV derived DNA sources from particular chromatin DNA loci. This understanding may enhance the accuracy and specificity of disease diagnosis in the future by focusing on specific sequences from patient's EV derived DNA.

While this study focuses primarily on FOXM1 and finds 103 FOXM1-LC3 ChIP loci and 25 FOXM1-chDNAs in evDNAs in particular, we believe that FOXM1-LC3

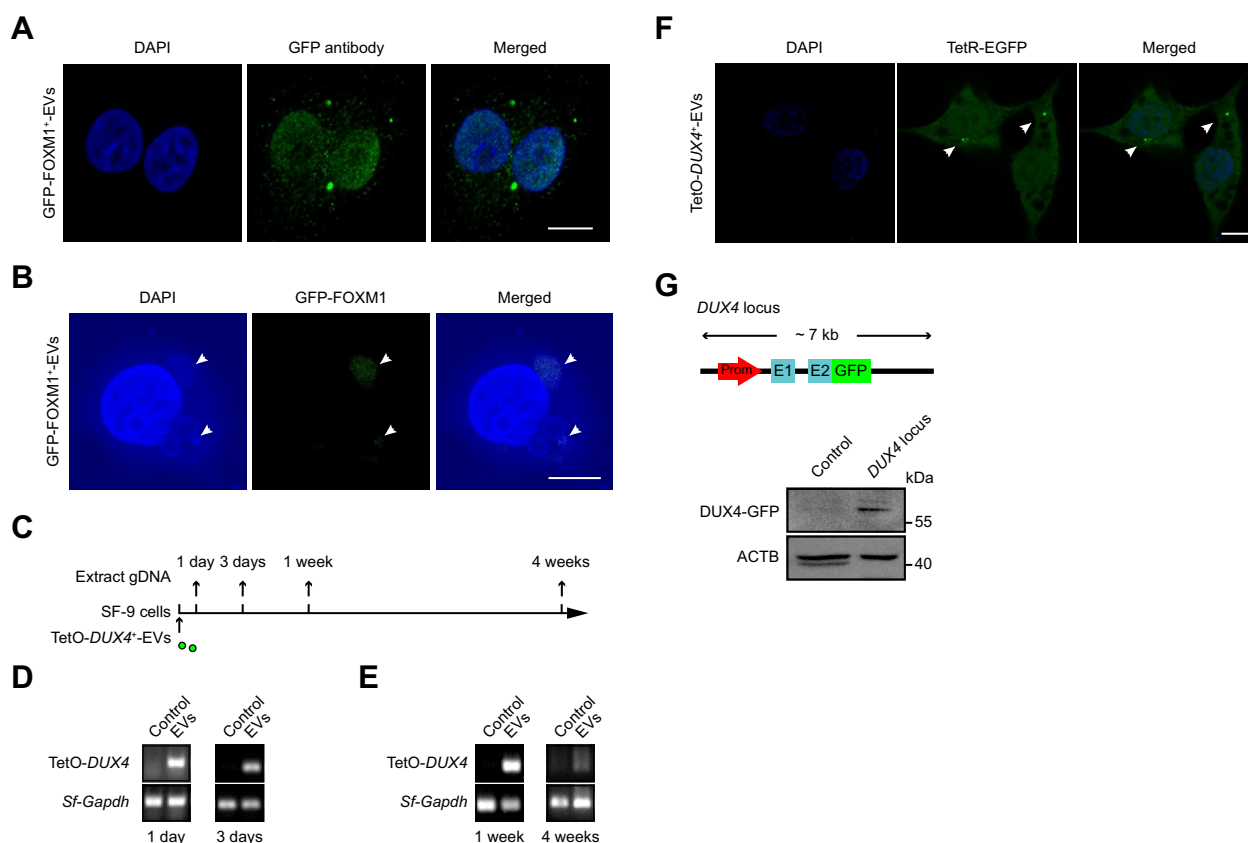


Figure 5. Transfer of FOXM1-chDNAs to recipient cells via EVs. (A) A549 cells were incubated 12 h with DIC-purified GFP-FOXM1⁺-EVs and immunostained by anti-GFP antibody for fluorescent imaging. (B) fluorescent imaging of A549 cells incubated 12 h with DIC-purified GFP-FOXM1⁺-EVs. The signals of DAPI were overexposed. The white arrows indicated GFP-FOXM1⁺-EVs. Scale bar: 10 μ m. (C) flow chart of A549^{TetO-DUX4} cells-derived EVs treated insect *spodoptera frugiperda* SF-9 cells. (D) SF-9 cells were treated as (C) and one or three days later the genomic DNA was extracted for PCR analyses of TetO-DUX4 DNA. (E) SF-9 cells were treated as (C) and one or four weeks later the genomic DNA was extracted for PCR analyses of TetO-DUX4 DNA. (F) A549-expressing TetR-EGFP cells were incubated 12 h with EVs that collected from starved-A549^{TetO-DUX4} cells. The white arrows indicated TetO-DUX4⁺-EVs. Scale bar: 10 μ m. (G) the last exon of DUX4 locus was fused with GFP cDNA before the stop codon (top). The modified DUX4 locus was amplified as FOXM1-chDNA3 and transfected into HEK293T cells for immunoblotting (bottom).

interaction is not a singular event confined to the nucleus. Our research has revealed that other forkhead box transcription factors, such as FOXA2 and FOXP2, also have the ability to interact with LC3 (Figure S6D). This suggests that these transcription factors may also have a part in determining evDNA sources from chromatin DNA. Furthermore, LC3 has been observed to interact with multiple transcription factors found in EVs through the use of mass spectrometry analysis [16,41]. This implies that these transcription factors may have a similar role to FOXM1 in directing evDNA from chromatin DNA. Typically, transcription factors are thought to bind to specific regions of chromosome DNA and regulate gene expression within the nucleus [63]. The findings of this study expand our understanding of transcription factors and offer a new perspective to explore their role in regulating the composition of EVs' DNA components. Additionally, further enrichment analysis of specific patient evDNA sequences can deduce the association between transcription factors and diseases and predict which transcription factors bind to those specific sequences, allowing for a deeper understanding of the pathogenesis or disease progression.

The FOXM1-chDNAs identified in this study can be classified as functional genes, telomeres, centromeres, and non-coding regions, suggesting potential impacts on recipient cells.

Notably, recent research has validated the horizontal transfer of telomere DNAs by EVs from antigen-presenting cells to T cells, indicating a role in rescuing T cells from senescence and promoting long-term immunological memory [9]. Our observation of TetO-DUX4 signaling in recipient cells treated with A549^{TetO-DUX4}-derived EVs, as well as phenotypic changes in cells transfected with PCR-amplified DNA from the DUX4 locus, further supports the notion that certain FOXM1-chDNAs may exhibit specific functions in recipient cells through horizontal gene transfer, ultimately regulating the extracellular microenvironment. Additionally, given that local cell-derived EVs can access the circulation, it is plausible that particular FOXM1-chDNAs could play a role in HGT in distant tissues. These hypotheses are currently under investigation in our laboratory.

FOXM1 functions as a transcription factor in nucleus to regulate gene expression [28]. However, this study has uncovered a new role for FOXM1 in directing certain chromatin DNA fragments to EVs. One outstanding question is how these specific fragments of chromatin DNA are broken down. Previous studies have shown that chromatin DNA can emerge in the cytoplasm via micronuclei and cytoplasmic chromatin fragment pathways [64], but these mechanisms cannot explain the specific breakdown of chromatin DNA.

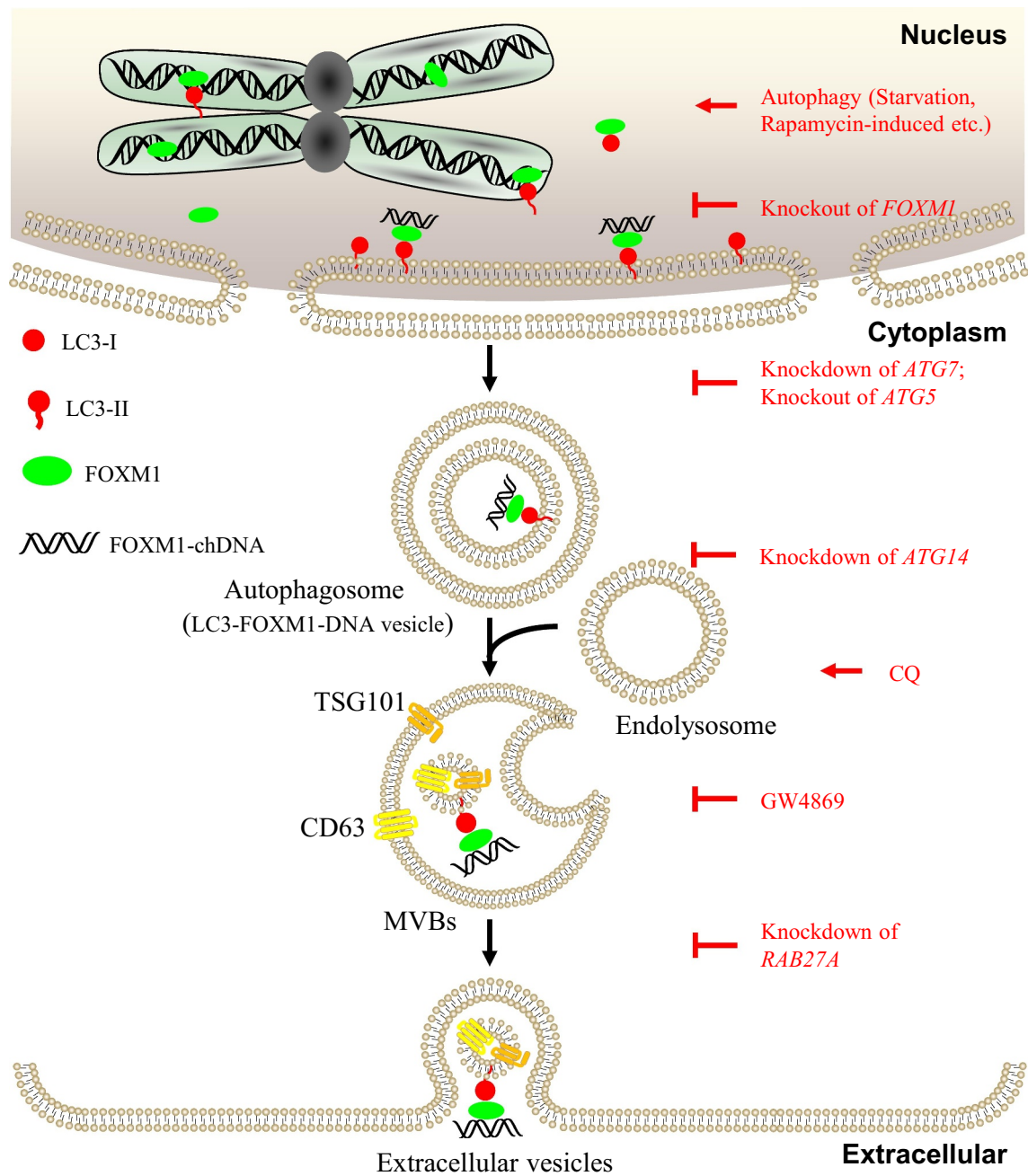


Figure 6. Schematic illustration of the FOXM1-chDNAs to EVs. FOXM1-bound chromatin DNA fragments (FOXM1-chDNAs), FOXM1, and LC3-II embedded on the nuclear membrane can form LC3-FOXM1-DNA vesicles in the cytoplasm during autophagy. EV-associated FOXM1-chDNAs are then secreted through MVB-involved SALI process. The potentiality that cytoplasmic chromatin fragments, FOXM1, and LC3-II may form LC3-FOXM1-DNA vesicles in the cytoplasm was not analyzed in this study. ATG7 [57], facilitates LC3 lipidation and translocation to the membrane of autophagosomes; ATG5 [58], mediates LC3 elongation on the membrane of autophagosomes; CD63 [54] and TSG101 [55], MVB specific markers; CQ, an autolysosome inhibitor [60]; GW4869 [61], a specific inhibitor of neutral sphingomyelinase for preventing intraluminal budding from the limiting membrane of the MVBs; ATG14 [18], promotes membrane tethering and fusion of autophagosomes to endolysosomes; RAB27A [62], a small GTPase that mediates fusion events between MVBs and the plasma membrane.

Although nuclear LC3 can translocate heterochromatin DNA to the cytoplasm via interaction with LMNB1 [10], the mechanism underlying the specific breaking off of chromatin DNA fragments from chromosomes remains unknown. Recent research has highlighted the Rec114, Mei4, and Mer2 complex as a machinery in cells that precisely controls DNA breakage [65], indicating that chromatin breakage could be precisely achieved. Further studies investigating FOXM1's interaction with the controlled DNA breakage machinery

will elucidate how relevant chromatin DNA fragments are produced with precision.

Materials and Methods

Cell culture

The human lung epithelial cell line A549 (ATCC, CCL-185) and human embryonal kidney cell line HEK293T (ATCC, CRL-3216)

were cultured in DMEM (Thermo Fisher 11,995,123) supplemented with 10% fetal bovine serum (FBS, Thermo Fisher 10,270,106), 100 U ml⁻¹ penicillin, and 100 µg ml⁻¹ streptomycin (Thermo Fisher 15,070,063). For starvation, cells were cultured in Earle's Balanced Salt Solution (EBSS, Thermo Fisher 24,010,043).

Plasmid constructs

The full length of human *FOXM1* (NM_202002.3) was amplified from pcDNA3.1-Flag-FOXM1 (PPL, BC006192) and cloned into the pCMV-Tag3B (Stratagene 211,173), pEGFP-C2 (Clontech, 6083-1), pBiFC-VN173 (Addgene 22,010; deposited by Chang-Deng Hu) and pcDNA3.1-RFP (HonorGene, HG-VPH003) vectors by one-step cloning to yield MYC-FOXM1, GFP-FOXM1, VN173-FOXM1 and RFP-FOXM1, respectively. The FOXM1 point mutations and truncations were obtained from these constructs by inverse PCR and self-ligation. The prokaryotic expression of FOXM1 was cloned into pET-25b (Novagen 69,753) vector.

The full length of human *LC3* (NM_022818.5) was amplified from pEGFP-LC3 (Addgene 87,872; deposited by Eiki Kominami) and cloned into the pBiFC-VC155 (Addgene 22,011; deposited by Chang-Deng Hu) and pGEX-4T2 (GE, 27-4581-01) vectors by one-step cloning to yield VC155-LC3 and GST-LC3, respectively. The LC3 point mutations and truncations were obtained from these constructs by inverse PCR and self-ligation. The Flag-FOXM1 and GFP-LC3 fragments were amplified and cloned into pLVX-IRES-Puro lentiviral expression vector (Clontech 632,183). The linear 72× M1-binding DNA were synthesized by TSINGKE Inc (Changsha, China).

Reagents and antibodies

The following reagents were used: chloroquine (CQ, Sigma-Aldrich, C6628), 3-methyladenine (3-MA, Sigma-Aldrich, M9281) and rapamycin (Sigma-Aldrich, V90093). GW4869 (MCE, HY-19363). Senescence β-Galactosidase Staining Kit (Beyotime, C0602). The following antibodies were used: LC3 (Proteintech, 146001AP; Cell Signaling Technology, 3868), FOXM1 (Santa Cruz Biotechnology, sc376471; Cell Signaling Technology 20,459), CD63 (Proteintech 25,682-1-AP), DYKDDDDK Tag (Cell Signaling Technology 14,793; Beyotime, AF0036), MYC-tag (Cell Signaling Technology, 2276; 2278), GFP-tag (Beyotime, AG279; Abcam, ab290), GFP-Trap (Chromotek, gta20), LMNB1/lamin B1 (Beyotime, AF1408), TUBB3/β-tubulin (Beyotime, AT809), GST (Beyotime, AF2299), ACTB/β-actin (Sigma-Aldrich, A5441), TSG101 (Beyotime, AF8259), RAB7 (Beyotime, AF2458), ATG7 (Ptm Bio, PTM-6267), ATG14 (Proteintech 194,911-AP), RAB27A (Beyotime, AG3056), HSPA8/HSC70 (Proteintech 106,541-AP), γ-H2AX (Abcam, ab81299), H3K9me3 (Beyotime, AF5707), histone H3 (Beyotime, AF0009), STING1 (Cell Signaling Technology 13,647), Phospho-STING1 (Ser366) (Cell Signaling Technology 50,907), SQSTM1 (Beyotime, AG4400), Goat Anti-Rabbit IgG H&L (Alexa Fluor® 488) antibody (Abcam, ab150077), Goat anti-Mouse IgG H&L (Cy3®) antibody (Abcam, ab97035).

Lentiviral packaging, infection and selection

To package lentivirus, HEK293T cells were co-transfected with the packaging vectors psPAX2 (Addgene 12,260; deposited by Didier Trono) and pMD.2 G (Addgene 12,259; deposited by Didier Trono), lentiviral constructs (such as pLVX-GFP-LC3, pLVX-Flag-FOXM1, pLKO.1-RAB27A shRNA (5'-GCT GCC AAT GGG ACA AAC ATA-3'), lentiCRISPR-FOXM1 sgRNA and lentiCRISPR-ATG5 sgRNA). Virus was filtered through a 0.45-µm filter (Millipore, SLHV033RB) and mixed with polybrene (Millipore, TR-1003-G) to a final concentration of 8 µg ml⁻¹. Subsequently, A549 or HEK293T cells were incubated with viral mix for 24 h and selected with 1 µg ml⁻¹ puromycin for about 1 week.

GST-affinity-isolation assay

HEK293T cells (5×10^6) were transfected with 5 µg plasmids (such as MYC-tagged FOXM1 and mutations) for 24 h and were lysed in the IP lysis buffer (50 mM Tris-HCl pH 7.4, 150 mM NaCl, 1% NP-40 [Sangon, 9016-45-9], 5 mM EDTA, 5 mM EGTA, 5% glycerol, containing 1× protease inhibitor cocktail [Beyotime, P1006]) and centrifuged at 12,000 × g for 10 min to obtain the supernatants. The supernatants were incubated with 30 µg bacterially purified GST-LC3 or truncated proteins and an additional 30 µl BeyoGold™ GST-tag Purification Resin (Beyotime, P2253; washed three times with PBS buffer) for 2 h at 4°C. The complex was washed 5 times with PBS buffer (containing 1 mM phenylmethylsulphonyl fluoride, PMSF [Thermo Fisher 36,978]). The proteins were eluted with 1× loading buffer by boiling for 10 min and analyzed by 10% SDS-PAGE followed by immunoblotting with anti-MYC antibody.

Immunofluorescence staining

Cells were treated as indicated and fixed in 4% paraformaldehyde in PBS for 40 min at 4°C, washed twice with TBST (0.1% Triton X-100 [Sangon, 9002-93-1] in TBS [50 mM Tris-HCl, pH 7.6, 150 mM NaCl]). Cells were then blocked in 5% BSA [Sangon, 9048-46-8] in TBS for 1 h at room temperature and incubated with primary antibodies in 5% BSA in TBS supplemented with 0.1% Tween 20 (Sangon, 9005-64-5; TBST) overnight at 4°C. Cells were washed 3 times with TBST, each for 5 min, followed by incubation with secondary antibodies in TBST (containing 5% BSA) for 1 h at room temperature. Cells were then washed 3 times in TBST and mounted with Mounting Medium with DAPI (Abcam, ab104139). Images were captured by FV1200 laser scanning microscopes (Olympus, Japan).

Immunoprecipitation

Cells (4×10^7) were lysed in the IP lysis buffer and centrifuged to obtain the supernatants. The supernatants were rotated with anti-IgG antibody (Sigma-Aldrich, 12-370) and additional Protein A/G magnetic beads (Thermo Scientific 88,802) for 4 h at 4°C. The supernatants were collected and incubated with antibody-conjugated Protein A/G magnetic

beads, and rotated at 4°C overnight. The immunoprecipitation was washed five times with PBS buffer (containing 1 mM PMSF), and boiled with 1 × loading buffer for 10 min. All samples were analyzed by western blotting.

Molecular docking

LC3 protein was obtained from PDB ID 2N9X and FOXM1-DBD was obtained from PDB ID 3G73. We confirmed that the LIR motif (317–320 aa) of FOXM1-DBD and F52 of LC3 mediated the interaction of FOXM1 and LC3. Therefore, ClusPro [66] (jobID = 701602) was first used for rigid docking under restricted conditions. After that, we separated the top1 structure to LC3 and FOXM1-DBD and use Rosetta Relax Application [67] to build the ensembles of LC3 and FOXM1-DBD. Then RosettaDock [35] was used to conduct flexible docking between the two ensembles for 10,000 times.

Nuclear and cytoplasmic components extract

Cells (4×10^7) were washed with PBS buffer and added 5 pellet volumes of CE buffer (10 mM HEPES, pH 7.6, 60 mM KCl, 1 mM EDTA, 0.075% NP-40, 1 mM DTT and 1 mM PMSF) to cell pellet (approximately 100 µL). Incubated on ice for 3 min. Spined the preparation using a microcentrifuge at 1000–1500 × g for 4 min. Removed the cytoplasmic extract from the pellet to a clean tube. Washed the nuclei with 100 µL of CE buffer without detergent. Be careful to resuspend the fragile nuclei gently. Spined the nuclei as above at 1000–1500 × g for 4 min. Added 1 pellet volume NE buffer (20 mM Tris-HCl, pH 7.5, 420 mM NaCl, 1.5 mM MgCl₂, 0.2 mM EDTA, 1 mM PMSF and 25% glycerol) to nuclear pellet (approximately 50 µL). Adjust the salt concentration to 400 mM using 5 M NaCl (add ~35 µL). Add an additional pellet volume of NE buffer. Vortex to resuspend the pellet. Incubate the extract on ice for 10 min. Vortex the mixture periodically to resuspend the pellet. Spin the CE and NE at maximum speed for 10 min to pellet any nuclei. Transfer the contents of the CE tube and NE tube separately to clean tubes. Add glycerol to the CE tube to 20%. Store at –70°C.

Recombinant protein expression and purification

All prokaryotic expression plasmids (pGEX-4T2 or pET-15b) were transformed into *Escherichia coli* BL21(DE3), inoculated in LB medium (containing Amp) and growth at 37°C until an optical density at 600 nm (OD₆₀₀) of 0.6 was reached, then isopropyl-β-D-thiogalactopyranoside (Sangon, 367-93-1; to a final concentration of 0.8 mM) was added. After growing for 12 h at 16°C, cells were pelleted and lysed in PBS buffer (containing 1 × protease inhibitor cocktail and 1 mM PMSF). The lysate was sonicated and centrifuged to obtain recombinant protein supernatants. The GST or GST-fused recombinant proteins were purified by BeyoGold™ GST-tag Purification Resin [68,69] (Beyotime, P2250) following the manufacturer's instruction. The His-fused recombinant proteins were purified by BeyoGold™ His-tag Purification Resin (Beyotime, P2233) following the manufacturer's instruction.

Chromatin immunoprecipitation (ChIP) assay

For FOXM1 or Flag-FOXM1 ChIP, cells (4×10^7) were cross-linked by formaldehyde and stopped by glycine. Cells were scraped and lysed with Nuclear Lysis Buffer (1% SDS, 10 mM EDTA, 50 mM Tris, pH 8.0, protease inhibitor) for 10 min on ice. The resulting extract was sonicated and taken 20% of samples as Input control. Other samples were performed immunoprecipitation. For LC3 or GFP-LC3, ChIP was performed as previously described [10]. All samples were reversed crosslinks and purified DNA to qPCR or sequence.

Isolation of MVBs by sucrose density gradient centrifugation

For the separation of MVBs, cells (4×10^7), cultured in DMEM with 10% FBS, were washed with ice-cold PBS and collected with a cell scraper. Centrifuge the cells at 300 g for 5 min at 4°C. Cell pellet was loosened using homogenization buffer (HB; 250 mM sucrose [Sangon, 57-50-1], 3 mM imidazole, pH 7.4, 1 mM EDTA, 0.03 mM cycloheximide [MCE, HY-12320], 10 mM iodoacetamide, 2 mM phenylmethylsulfonyl fluoride (PMSF), and 1 × cocktail inhibitor). Centrifuge at 1300 g for 10 min at 4°C. The supernatants were discarded, and the pellet was gently resuspended with a wide-cut tip in three times the pellet volume of HB. The suspension was passed through a 1-ml syringe two to 10 times. Dilute the homogenate in HB (1 part homogenate to 0.7 parts HB). Centrifuge at 2000 g for 10 min at 4°C. Collect the supernatants and centrifuge again. Carefully collect the supernatants (termed the post-nuclear supernatants [PNS]) from the second centrifugation.

Sucrose density solutions were prepared before use to generate discontinuous step (10%–62%) gradients. The PNS was carefully added to the top of sucrose density gradients (10%–62%) in a centrifugation tube. The samples were subjected to ultracentrifugation at 140,000 g for 15 h at 4°C using a SW28 TI Swinging Bucket rotor (*k* factor of 246, Beckman Coulter). Five individual fractions of 1 mL were collected from the top of the gradient. For immunoblotting, each individual 1 mL fraction was transferred to new ultracentrifugation tubes, diluted 25-fold in PBS and subjected to ultracentrifugation at 140,000 × g for 4 h at 4°C using a SW28 TI Swinging Bucket rotor. The resulting pellets were lysed in cell lysis buffer for 10 min on ice. For DNA extraction, the resulting pellets were extracted by QIAamp DNA Mini Kit (Qiagen 51,304) following the manufacturer's instruction.

Rapid method for the immune-purification of MVBs (IP-MVBs)

Cells were quickly washed twice with PBS and then scraped in one ml of KPBS (130 mM KCl, 10 mM KH₂PO₄, pH 7.25 was adjusted with KOH) and centrifuged at 1,000 g for 2 min at 4°C. Pelleted cells were resuspended in 950 µL, and 25 µL (equivalent to 2.5% of the total cells) was reserved for further processing of the whole-cell fraction. The remaining cells were gently homogenized with 20 strokes of a 2 ml

homogenizer (Beyotime, E1901). The homogenate was centrifuged at 1,000 g for 2 min at 4°C. The magnetic beads were incubated with anti-CD63 antibody for 1 h. Subsequently, the supernatants were incubated with the magnetic beads for an additional h at 4°C. Immunoprecipitates were gently washed three times with KPBS on a magnetic rack. For immunoblotting, the samples were lysed with IP buffer and analyzed by SDS-PAGE. For DNA extraction, the samples were extracted by QIAamp DNA Mini Kit following the manufacturer's instruction.

Protein and DNA extraction from extracellular vesicles

The EV pellets were lysed by urea lysis buffer (100 mM NaH₂PO₄, 10 mM Tris-HCl pH 8.0, 8 M urea [Sangon, 57-13-6], 10 mM imidazole, containing 1 × protease inhibitor cocktail) and analyzed by immunoblotting [16]. The extracellular vesicle DNAs (evDNAs) were extracted by QIAamp DNA Mini Kit following the manufacturer's instruction.

Direct immunoaffinity capture (DIC) of EVs

DIC assays of EVs were performed as described [1]. Briefly, the cell-conditioned medium was collected as described above. After ultracentrifugation at 15,000 × g for 40 min, the supernatants were incubated with magnetic beads directly conjugated to FOXM1 antibody or GFP-Trap beads for 16 h. After incubation, all beads were washed for immunoblotting or evDNAs extraction.

Biotinylated DNA affinity-isolation assay

For the biotinylation of FOXM1-chDNA3 (chr4: 190179246–190180026), the 979 bp biotinylated DUX4 DNA was prepared by PCR amplification using a pair of 5'biotinylated primers: 5'-biotin-ACT CCA CTC CGC GGA GAA-3' and 5'-biotin-CTT GTC AAG GTT TGG CTT ATA GG-3'. The PCR products were purified by Universal DNA Purification Kit (TIANGEN, DP214) following the manufacturer's instruction.

For DNA-affinity-isolation, A549 cells were lysed in IP lysis buffer and centrifuged to obtain the supernatants. The supernatants were incubated with 500 ng biotinylated DUX4 DNA for 1 h and additional 50 μl streptavidin beads for another 1 h at room temperature. The complex was washed 5 times with IP lysis buffer. The proteins were eluted with 1 × loading buffer by boiling for 10 min and analyzed by 10% SDS-PAGE followed by immunoblotting with primary antibodies [70].

Electrophoretic mobility shift assays (EMSA)

EMSA was performed as previously described [71]. Briefly, His-FOXM1 protein (10 μg) were incubated with the FAM-labeled DNA probe (50 nM) containing putative FOXM1 sites in binding buffer (20 mM Tris-Cl, 50 mM KCl, 10% glycerol, 0.5 mM EDTA, 0.2 mM DTT, pH 7.6) for 30 min on ice. The purified GST-LC3 protein was used to detect supershift.

CRISPR-Cas9-mediated knockout of FOXM1 and ATG5

To obtain A549^{FOXM1}^{-/-} or A549^{ATG5}^{-/-} cell line, we designed their sgRNA using <http://crispr.mit.edu/>. The sgRNA (5'-GAT GGC CAC TAC TTG CGT GT-3') targeted to FOXM1 or sgRNA (5'-GAT GGA CAG TTG CAC ACA CT-3') targeted to ATG5 was cloned into the lentiCRISPR v2 vector (Addgene 52,961; deposited by Feng Zhang). FOXM1 sgRNA or ATG5 sgRNA lentivirus were packaged and transduced to A549 cells. The transduced cells were selected with 1 μg ml⁻¹ puromycin for 2 weeks to obtain the FOXM1^{-/-} or ATG5^{-/-} cells.

ChIP sequencing, evDNA sequencing, bioinformatics analysis, RT-qPCR

For sequencing, ChIP and evDNA samples were prepared as described previously [72]. The ChIP and evDNA were purified and used for constructing sequencing libraries with a NEBNext Ultra DNA Library Prep Kit for Illumina (New England Biolabs, E7370L). The library quantifications were assessed on the Agilent Bioanalyzer 2100 system. The library preparations were sequenced on an Illumina HiSeq platform and 50-bp single-end reads or 150-bp paired-end reads were generated.

For bioinformatics analysis, the following pipeline was used for analysis of all sequence data sets. Firstly, fastp (version 0.20.0, parameter: “-q 15 -u 40 -n 6 -l 15”) [73] was used to trim adaptors and low-quality reads. Then, we evaluated the quality of NGS short reads by searching them on the FastQC (version 0.11.8) program (<http://www.bioinformatics.babraham.ac.uk/projects/fastqc>). Thirdly, the remaining reads were aligned to human genome hg38 by bwa mem (version 0.7.17, parameter: “-t 20”) [74], since ChIP-Seq and evDNA-Seq interrupted fragments were usually small and the percentage of unique sequences in the total number of sequences was the focus of attention. Finally, peak calling of the aligned reads was made using macs3 (version 3.0.0a6, parameter: “-f BAM -g hs -p 0.1 -B”) [75], and peaks were annotated using the R/Bioconductor package ChIPseeker [76]. Browser views of peaks are shown using Integrated Genomics Viewer (IGV; broadinstitute.org/igv) [77].

For qPCR, the following primers were used for qPCR analyses of chromatin loci. FOXM1-chDNA1 (chr18): forward, 5'-TGA TCA CCC AGG AGA CGG-3'; reverse, 5'-CTT GGG TGA TCA GTG GCG AG-3'. FOXM1-chDNA2 (chr9): forward, 5'-CTG CAA AAT GGA CCA ATC AGC-3'; reverse, 5'-AAG ATG GTG TGT CCG GAA TTT G-3'. FOXM1-chDNA3 (chr4): forward, 5'-TCA CAA GCC CCC TGT AGG-3'; reverse, 5'-TCC AAC TCT TGC CTG GTC TC-3'.

DNA fluorescence in situ hybridization (FISH)

DNA-FISH probes were constructed by Exon Biotechnology Inc (Guangzhou, China). The probes covered genomic regions (hg38) used in this study was as follow: chr18: 103010–113570 (chr18_FOXM1-chDNA1_10 Kb). For fluorescence *in situ* hybridization assay, DNA FISH was performed as described [78]. Briefly, coverslips containing fixed and permeabilized

cells were quenched by 3% H₂O₂, followed by dehydration in 70%, 85%, and 100% ethanol for 1 min each. FISH probe (chr18_FOXM1-chDNA1_10 Kb) was added onto a glass slide, and lower the coverslips onto the slide slowly. Place the slides with samples to be hybridized in a heating block at 85°C for 5 min, and then 37°C for 20 h. The slide was then removed, and the sample was washed with Wash Buffer (1 X, preheated to 73°C) for 2 min. Added blocking buffer onto the hybridized samples and incubated at 37°C for 30 min. Added primary antibody onto coverslip and incubated at 37°C for 30 min. The sample was washed with Wash Buffer (1 X, preheated to 45°C) for 5 min. Added secondary antibody onto coverslip and incubated at 37°C for 30 min. Wash coverslip in Wash Buffer (1×) three times at 45°C for 5 min. Re-wash once with PBS. Preparation of TSA solution at TSA: 0.15% H₂O₂: TSA amplification buffer = 1:5:500–1:10:1000. Add TSA solution to coverslip and incubate 5–15 min at RT. Wash coverslip in Wash Buffer (1 X) three times for 30 min. Mount coverslip with Anti-fade Fluorescence Mounting Medium (with DAPI, Abcam, ab104139).

CRISPR-Cas9-mediated knock-in of a TetO array (96×) for visualization of FOXM1-chDNAs

To obtain a TetO-knockin cell line, we designed a pair of gRNAs using <http://crispr.mit.edu/>. The pair of gRNAs (5'-CAC CTG GGT GAT CAG AGC AA-3' and 5'-TCT AGG CTT TGG CCT ACA GG-3') bound to FOXM1-chDNA1 or gRNAs (5'-GCA GGC AGA GCG TAA GCA AA-3' and 5'-GGA CAC ACG TTT AAT CGA GT-3') bound to FOXM1-chDNA3 was cloned into the p×335vector (Addgene 42,335; deposited by Feng Zhang) before the gRNA scaffold. Furthermore, we designed two donor plasmids that contain the TetO array (96×) flanked by 500-bp homology arms of the FOXM1-chDNAs in the pSP2-96-merTetO-EFS-BLaR vector (Addgene 118,713; deposited by Huimin Zhao). The primers (5'-CCC TTT CGT CTT CAA GAA TTC CAT CAC CTG GGT GAT CAG TGT AGA-3', 5'-ACC CAT TCC TAG GGC GAA TTC GCT CTC TGA TCA CCC AGG TGA T-3'; 5'-GCG CTGC TAG CTT AAG GTA CCA GCG TAG GCC AAA GCC TAG AC-3', 5'-CCC AGA TCT ATC GAT GGT ACC CTT GTC TAG GAT CTG CCT ACA GGG-3') were synthesized and amplified homology arms of the FOXM1-chDNA1. The primers (5'- CCC TTT CGT CTT CAA GAA TTC CCT GTA GGC AAG CCT ACA CAA GT-3', 5'-ACC CAT TCC TAG GGC GAA TTC AGC GCT TAC GCT CTG CCT G-3'; 5'-GCG CTG CTA GCT TAA GGT ACC GAC CGA TTA AAC GTG TGT CCT TT-3', 5'-CCC AGA TCT ATC GAT GGT ACC GTT TTT TCC TTT AAG ACT TAT GTA ATG AAT T-3') were synthesized and amplified homology arms of the FOXM1-chDNA3. The paired gRNAs and donor plasmids were co-transfected into A549 cells. Blasticidin (10 µg/ml) selection was started 1 day after transfection. Three weeks after blasticidin selection, TetO-knockin cell clones were transplanted into 24-well plates. Cells were collected from 24-well plates and extracted genomic DNA (gDNA) for genotyping.

For FOXM1-chDNAs loci visualization, the TetO-knockin cells were transiently expressed with TetR-EGFP.

Cells were fixed in 4% paraformaldehyde and mounted with Mounting Medium with DAPI (Abcam, ab104139). Images were captured by FV1200 laser scanning microscopes (Olympus, Japan). For qPCR, the following primers were used for qPCR analyses of knock-in of FOXM1-chDNAs. TetO-telomere DNA (FOXM1-chDNA1 locus): forward, 5'-GAA GAC TAC AGC GTC GCC AG-3'; reverse, 5'-CGC GAC GAT ACA AGT CAG GT-3'. TetO-DUX4 DNA (FOXM1-chDNA3 locus): forward, 5'-TCT GAA GAC TAC AGC GTC GC-3'; reverse, 5'-ACA CAT AAC CAG AGG GCA GC-3'.

Extracellular vesicle isolation

Cells seeded in 150-mm culture dishes at approximately 80% confluence were incubated with serum-free DMEM for 1 day or 2 days. Cell viability was assessed using trypan blue and only >95% viability was used for EVs isolation. The cell-conditioned medium was collected by sequential ultracentrifugation [1,16]. Briefly, the medium was first subjected to a centrifugation at 400 × g for 10 min to remove cells. Next, the supernatant was centrifuged at 2,000 × g for 20 min to remove debris and apoptotic bodies. Then, the supernatant was centrifuged at 15,000 × g for 40 min to obtain large EVs. The resulting large EVs pellet was resuspended in a large volume of PBS buffer followed by ultracentrifugation at 15,000 × g for 40 min to wash the sample. To remove any remaining any large EVs, the media supernatant from the first 15,000 × g step was passed through a 0.22-µm pore PES filter (Millipore, SLGP033NS). This supernatant (pre-cleared medium) was next subjected to ultracentrifugation at 120,000 × g for 4 h in a SW 28 Ti Swinging-Bucket Rotor (Beckman Coulter, Fullerton, CA) to sediment small EVs. The crude small EVs pellet was resuspended in a large volume of PBS followed by ultracentrifugation at 120,000 × g for 4 h to wash the sample. All following centrifugation steps were performed at 4°C. Notably, for the comparison of EVs in different conditions, the results must be corrected by total cell number or total protein concentration to eliminate differences in cell seeding.

siRNA-mediated silencing

All siRNA were designed and synthesized by GenePharma (Shanghai, China). FOXM1 siRNA was synthesized as follows: #1 5'-UUU CAC UUG GGG CAU UUU GAA-3'; #2 5'-UGG UUA AUA AUC UUG AUC CCA-3' and #3 5'-GGA CCA CUU UCC CUA CUU UTT-3'. ATG7 siRNA: #1 5'-GCC AGU GGG UUU GGA UCA ATT-3' and #2 5'-GCC UCU CUA UGA GUU UGA ATT-3'. ATG14 siRNA: #1 5'-GGG AGA GGU UUA UCG ACA ATT -3' and #2 5'-GGG UCU GUG ACG AUC ACA ATT-3'. Negative control: 5'-UUC UCC GAA CGU GUC ACG UTT-3'. For siRNA-mediated silencing, cells were transiently transfected with siRNA (50 nM) using Lipofectamine 2000 (Life Technologies 11,668,019) according to the manufacturer's protocols.

Proteinase K protection assay

The EVs were incubated in either PBS or 10 µg/ml proteinase K (Beyotime, ST532) in PBS, with or without the presence of 0.1% Triton X-100 for 1 h at 37°C. The assay was stopped by addition of 5 X Loading Buffer, incubation at 95°C. All samples were analyzed by western blotting.

Statistical analysis

All the statistical analyses were performed using GraphPad Prism 5 software. Student's *t*-test was used for comparison between two groups. One-way ANOVA with Dunnett's post-test analysis was performed to evaluate differences between groups of three or more. Significance was considered when the *P*-value was less than 0.05.

Acknowledgements

We thank Dr. Zhuoxian Rong of Central South University for help with construction of FOXM1 knockout A549 cell line by CRISPR-Cas9 technology; thank Dr. Jianhui Jiang of Hunan University for help with confocal microscopy; thank Dr. Feng Yu of Hunan University for sharing SF-9 cell line; thank Ms. Yan Chen, Dr. Xiaoqin Huang and Dr. Li Yu of Hunan University for scientific discussion and experimental assistance during the manuscript revision.

Disclosure statement

No potential conflict of interest was reported by the author(s).

Funding

The work was supported by the The National Natural Science Foundation of China [81773169]; China Changsha Development and Reform Commission "Innovation platform construction program" [2018-216]; China Changsha Development and Reform Commission "Mass entrepreneurship and innovation program" [2018-68].

Data availability statement

All data and materials are available upon request. The ChIP-seq and evDNA-seq data are deposited under the following link: GSE216672 (<https://www.ncbi.nlm.nih.gov/geo/query/acc.cgi?acc=GSE216672>).

ORCID

Yongjun Tan  <http://orcid.org/0000-0003-1367-1738>

References

- Jeppesen DK, Fenix AM, Franklin JL, et al. Reassessment of exosome Composition. *Cell*. 2019 Apr 4;177(2):428–445 e18. doi: [10.1016/j.cell.2019.02.029](https://doi.org/10.1016/j.cell.2019.02.029)
- van Niel G, D'Angelo G, Raposo G. Shedding light on the cell biology of extracellular vesicles. *Nat Rev Mol Cell Biol*. 2018 Apr;19(4):213–228. doi: [10.1038/nrm.2017.125](https://doi.org/10.1038/nrm.2017.125)
- Sina AA, Lin TY, Vaidyanathan R, et al. Methylation dependent gold adsorption behaviour identifies cancer derived extracellular vesicular DNA. *Nanoscale Horiz*. 2020 Sep 1;5(9):1317–1323. doi: [10.1039/D0NH00258E](https://doi.org/10.1039/D0NH00258E)
- Elzanowska J, Semira C, Costa-Silva B. DNA in extracellular vesicles: biological and clinical aspects. *Mol Oncol*. 2020 Aug 7;15(6):1701–1714. doi: [10.1002/1878-0261.12777](https://doi.org/10.1002/1878-0261.12777)
- Douanne N, Dong G, Amin A, et al. Leishmania parasites exchange drug-resistance genes through extracellular vesicles. *Cell Rep*. 2022 Jul 19;40(3):111121. doi: [10.1016/j.celrep.2022.111121](https://doi.org/10.1016/j.celrep.2022.111121)
- Soucy SM, Huang J, Gogarten JP. Horizontal gene transfer: building the web of life. *Nat Rev Genet*. 2015 Aug;16(8):472–482. doi: [10.1038/nrg3962](https://doi.org/10.1038/nrg3962)
- Cai J, Wu G, Jose PA, et al. Functional transferred DNA within extracellular vesicles. *Exp Cell Res*. 2016 Nov 15;349(1):179–183. doi: [10.1016/j.yexcr.2016.10.012](https://doi.org/10.1016/j.yexcr.2016.10.012)
- Kawamura Y, Sanchez Calle A, Yamamoto Y, et al. Extracellular vesicles mediate the horizontal transfer of an active LINE-1 retrotransposon. *J Extracell Vesicles*. 2019;8(1):1643214. doi: [10.1080/20013078.2019.1643214](https://doi.org/10.1080/20013078.2019.1643214)
- Lanna A, Vaz B, D'Ambra C, et al. An intercellular transfer of telomeres rescues T cells from senescence and promotes long-term immunological memory. *Nat Cell Biol*. 2022 Sep 15;24(10):1461–1474. doi: [10.1038/s41556-022-00991-z](https://doi.org/10.1038/s41556-022-00991-z)
- Dou Z, Xu C, Donahue G, et al. Autophagy mediates degradation of nuclear lamina. *Nature*. 2015 Nov 5;527(7576):105–109. doi: [10.1038/nature15548](https://doi.org/10.1038/nature15548)
- Lee YK, Lee JA. Role of the mammalian ATG8/LC3 family in autophagy: differential and compensatory roles in the spatiotemporal regulation of autophagy. *BMB Rep*. 2016 Aug;49(8):424–430. doi: [10.5483/BMBRep.2016.49.8.081](https://doi.org/10.5483/BMBRep.2016.49.8.081)
- Oldenburg AR, Collas P. Mapping nuclear lamin-Genome Interactions by chromatin immunoprecipitation of nuclear Lamins. *Methods Mol Biol*. 2016;1411:315–324.
- Tanida I, Ueno T, Kominami E. LC3 and Autophagy. *Methods Mol Biol*. 2008;445:77–88.
- Itakura E, Kishi-Itakura C, Mizushima N. The hairpin-type tail-anchored SNARE syntaxin 17 targets to autophagosomes for fusion with endosomes/lysosomes. *Cell*. 2012 Dec 7;151(6):1256–1269. doi: [10.1016/j.cell.2012.11.001](https://doi.org/10.1016/j.cell.2012.11.001)
- New J, Thomas SM. Autophagy-dependent secretion: mechanism, factors secreted, and disease implications. *Autophagy*. 2019 Oct;15(10):1682–1693. doi: [10.1080/15548627.2019.1596479](https://doi.org/10.1080/15548627.2019.1596479)
- Leidal AM, Huang HH, Marsh T, et al. The LC3-conjugation machinery specifies the loading of RNA-binding proteins into extracellular vesicles. *Nat Cell Biol*. 2020 Feb;22(2):187–199. doi: [10.1038/s41556-019-0450-y](https://doi.org/10.1038/s41556-019-0450-y)
- Solvik TA, Nguyen TA, Tony Lin YH, et al. Secretory autophagy maintains proteostasis upon lysosome inhibition. *J Cell Bio*. 2022 Jun 6;221(6). doi: [10.1083/jcb.202110151](https://doi.org/10.1083/jcb.202110151)
- Diao J, Liu R, Rong Y, et al. ATG14 promotes membrane tethering and fusion of autophagosomes to endolysosomes. *Nature*. 2015 Apr 23;520(7548):563–566. doi: [10.1038/nature14147](https://doi.org/10.1038/nature14147)
- Kalluri R, LeBleu VS. The biology, function, and biomedical applications of exosomes. *Science*. 2020 Feb 7;367(6478). doi: [10.1126/science.aau6977](https://doi.org/10.1126/science.aau6977)
- Leidal AM, Debnath J. LC3-dependent extracellular vesicle loading and secretion (LDELS). *Autophagy*. 2020 Jun;16(6):1162–1163. doi: [10.1080/15548627.2020.1756557](https://doi.org/10.1080/15548627.2020.1756557)
- Gruenbaum Y, Wilson KL, Harel A, et al. Review: nuclear lamins—structural proteins with fundamental functions. *J Struct Biol*. 2000 Apr;129(2–3):313–323. doi: [10.1006/jsbi.2000.4216](https://doi.org/10.1006/jsbi.2000.4216)
- Costa RH, Kalinichenko VV, Holterman AX, et al. Transcription factors in liver development, differentiation, and regeneration. *Hepatology*. 2003 Dec;38(6):1331–1347. doi: [10.1016/j.hep.2003.09.034](https://doi.org/10.1016/j.hep.2003.09.034)
- Fu Z, Malureanu L, Huang J, et al. Plk1-dependent phosphorylation of FoxM1 regulates a transcriptional programme required for mitotic progression. *Nat Cell Biol*. 2008 Sep;10(9):1076–1082. doi: [10.1038/ncb1767](https://doi.org/10.1038/ncb1767)
- Tan Y, Raychaudhuri P, Costa RH. Chk2 mediates stabilization of the FoxM1 transcription factor to stimulate expression of DNA repair genes. *Mol Cell Biol*. 2007 Feb;27(3):1007–1016. doi: [10.1128/MCB.01068-06](https://doi.org/10.1128/MCB.01068-06)
- Song IS, Jeong YJ, Jeong SH, et al. FOXM1-induced PRX3 regulates stemness and survival of colon cancer cells via maintenance

- of mitochondrial function. *Gastroenterology*. 2015 Oct;149(4):1006–16 e9. doi: [10.1053/j.gastro.2015.06.007](https://doi.org/10.1053/j.gastro.2015.06.007)
- [26] Xie Z, Tan G, Ding M, et al. Foxm1 transcription factor is required for maintenance of pluripotency of P19 embryonal carcinoma cells. *Nucleic Acids Res*. 2010 Dec;38(22):8027–8038. doi: [10.1093/nar/gkq715](https://doi.org/10.1093/nar/gkq715)
- [27] Li D, Wei P, Peng Z, et al. The critical role of dysregulated FOXM1-PLAUR signaling in human colon cancer progression and metastasis. *Clin Cancer Res*. 2013 Jan 1;19(1):62–72. doi: [10.1158/1078-0432.CCR-12-1588](https://doi.org/10.1158/1078-0432.CCR-12-1588)
- [28] Sanders DA, Gormally MV, Marsico G, et al. FOXM1 binds directly to non-consensus sequences in the human genome. *Genome Biol*. 2015 Jun 23;16(1):130. doi: [10.1186/s13059-015-0696-z](https://doi.org/10.1186/s13059-015-0696-z)
- [29] Marceau AH, Brison CM, Nerli S, et al. An order-to-disorder structural switch activates the FoxM1 transcription factor. *Elife*. 2019 May 28;8:e46131. doi: [10.7554/eLife.46131](https://doi.org/10.7554/eLife.46131)
- [30] Liu C, Barger CJ, Karpf AR. FOXM1: a multifunctional oncoprotein and emerging therapeutic target in ovarian cancer. *Cancers (Basel)*. 2021 Jun 19;13(12):3065. doi: [10.3390/cancers13123065](https://doi.org/10.3390/cancers13123065)
- [31] Hu CD, Kerppola TK. Simultaneous visualization of multiple protein interactions in living cells using multicolor fluorescence complementation analysis. *Nat Biotechnol*. 2003 May;21(5):539–545. doi: [10.1038/nbt816](https://doi.org/10.1038/nbt816)
- [32] Birgisdottir AB, Lamark T, Johansen T. The LIR motif - crucial for selective autophagy. *J Cell Sci*. 2013 Aug 1;126(Pt 15):3237–3247. doi: [10.1242/jcs.126128](https://doi.org/10.1242/jcs.126128)
- [33] Johansen T, Lamark T. Selective Autophagy: ATG8 Family Proteins, LIR Motifs and Cargo Receptors. *J Mol Biol*. 2020 Jan 3;432(1):80–103. doi: [10.1016/j.jmb.2019.07.016](https://doi.org/10.1016/j.jmb.2019.07.016)
- [34] Sentelle RD, Senkal CE, Jiang WH, et al. Ceramide targets autophagosomes to mitochondria and induces lethal mitophagy. *Nat Chem Biol*. 2012 Oct;8(10):831–838. doi: [10.1038/nchembio.1059](https://doi.org/10.1038/nchembio.1059)
- [35] Chaudhury S, Berrondo M, Weitzner BD, et al. Benchmarking and analysis of protein docking performance in Rosetta v3.2. *PLoS One*. 2011;6(8):e22477. doi: [10.1371/journal.pone.0022477](https://doi.org/10.1371/journal.pone.0022477)
- [36] Littler DR, Alvarez-Fernandez M, Stein A, et al. Structure of the FoxM1 DNA-recognition domain bound to a promoter sequence. *Nucleic Acids Res*. 2010 Jul;38(13):4527–4538. doi: [10.1093/nar/gkq194](https://doi.org/10.1093/nar/gkq194)
- [37] Kuang Y, Ma K, Zhou C, et al. Structural basis for the phosphorylation of FUNDC1 LIR as a molecular switch of mitophagy. *Autophagy*. 2016 Dec;12(12):2363–2373. doi: [10.1080/15548627.2016.1238552](https://doi.org/10.1080/15548627.2016.1238552)
- [38] Pankiv S, Clausen TH, Lamark T, et al. p62/SQSTM1 binds directly to Atg8/LC3 to facilitate degradation of ubiquitinated protein aggregates by autophagy. *J Biol Chem*. 2007 Aug 17;282(33):24131–24145. doi: [10.1074/jbc.M702824200](https://doi.org/10.1074/jbc.M702824200)
- [39] Ivanov A, Pawlikowski J, Manoharan I, et al. Lysosome-mediated processing of chromatin in senescence. *J Cell Bio*. 2013 Jul 8;202(1):129–143. doi: [10.1083/jcb.201212110](https://doi.org/10.1083/jcb.201212110)
- [40] Gluck S, Guey B, Gulen MF, et al. Innate immune sensing of cytosolic chromatin fragments through cGAS promotes senescence. *Nat Cell Biol*. 2017 Sep;19(9):1061–1070. doi: [10.1038/ncb3586](https://doi.org/10.1038/ncb3586)
- [41] Hoshino A, Kim HS, Bojmar L, et al. Extracellular Vesicle and Particle Biomarkers Define Multiple Human Cancers. *Cell*. 2020 Aug 20;182(4):1044–1061 e18. doi: [10.1016/j.cell.2020.07.009](https://doi.org/10.1016/j.cell.2020.07.009)
- [42] Moller A, Lobb RJ. The evolving translational potential of small extracellular vesicles in cancer. *Nat Rev Cancer*. 2020 Sep 21;20(12):697–709. doi: [10.1038/s41568-020-00299-w](https://doi.org/10.1038/s41568-020-00299-w)
- [43] Gao Y, Qin Y, Wan C, et al. Small Extracellular Vesicles: A Novel Avenue for Cancer Management. *Front Oncol*. 2021;11:638357. doi: [10.3389/fonc.2021.638357](https://doi.org/10.3389/fonc.2021.638357)
- [44] Yoshioka Y, Konishi Y, Kosaka N, et al. Comparative marker analysis of extracellular vesicles in different human cancer types. *J Extracell Vesicles*. 2013;2:eCollection. doi: [10.3402/jev.v2i0.20424](https://doi.org/10.3402/jev.v2i0.20424)
- [45] Abmayr SM, Yao T, Parmely T, et al. Preparation of nuclear and cytoplasmic extracts from mammalian cells. *Curr Protoc Mol Biol*. 2006;75(1):Aug;Chapter 12:Unit 12.1. doi: [10.1002/0471142727.mb1201s75](https://doi.org/10.1002/0471142727.mb1201s75)
- [46] Wang Y, Wang M, Djekidel MN, et al. eccDnas are apoptotic products with high innate immunostimulatory activity. *Nature*. 2021 Nov;599(7884):308–314. doi: [10.1038/s41586-021-04009-w](https://doi.org/10.1038/s41586-021-04009-w)
- [47] Liu H, Tian Y, Xue C, et al. Analysis of extracellular vesicle DNA at the single-vesicle level by nano-flow cytometry. *J Extracell Vesicles*. 2022 Apr;11(4):e12206. doi: [10.1002/jev.12206](https://doi.org/10.1002/jev.12206)
- [48] Bonsel E, Lavieu G. Content release of extracellular vesicles in a cell-free extract. *FEBS Lett*. 2019 Aug;593(15):1983–1992. doi: [10.1002/1873-3468.13472](https://doi.org/10.1002/1873-3468.13472)
- [49] Tasan I, Sustackova G, Zhang L, et al. CRISPR/Cas9-mediated knock-in of an optimized TetO repeat for live cell imaging of endogenous loci. *Nucleic Acids Res*. 2018;46(17):e100. doi: [10.1093/nar/gky501](https://doi.org/10.1093/nar/gky501)
- [50] Hendrickson PG, Dorais JA, Grow EJ, et al. Conserved roles of mouse DUX and human DUX4 in activating cleavage-stage genes and MERVL/HERVL retrotransposons. *Nat Genet*. 2017 Jun;49(6):925–934. doi: [10.1038/ng.3844](https://doi.org/10.1038/ng.3844)
- [51] Chew GL, Campbell AE, De Neef E, et al. DUX4 Suppresses MHC class I to promote cancer immune evasion and resistance to checkpoint blockade. *Dev Cell*. 2019 Sep 9;50(5):658–671 e7. doi: [10.1016/j.devcel.2019.06.011](https://doi.org/10.1016/j.devcel.2019.06.011)
- [52] de Araujo ME, Lamberti G, Huber LA. Homogenization of Mammalian Cells. *Cold Spring Harb Protoc*. 2015 Nov 2;2015(11):1009–1012. doi: [10.1101/pdb.prot083436](https://doi.org/10.1101/pdb.prot083436)
- [53] Shearer LJ, Petersen NO. Distribution and co-localization of endosome markers in cells. *Heliyon*. 2019 Sep;5(9):e02375. doi: [10.1016/j.heliyon.2019.e02375](https://doi.org/10.1016/j.heliyon.2019.e02375)
- [54] Piper RC, Katzmann DJ. Biogenesis and function of multivesicular bodies. *Annu Rev Cell Dev Biol*. 2007;23(1):519–547. doi: [10.1146/annurev.cellbio.23.090506.123319](https://doi.org/10.1146/annurev.cellbio.23.090506.123319)
- [55] Nabhan JF, Hu R, Oh RS, et al. Formation and release of arrestin domain-containing protein 1-mediated microvesicles (ARMMs) at plasma membrane by recruitment of TSG101 protein. *Proc Natl Acad Sci U S A*. 2012 Mar 13;109(11):4146–4151. doi: [10.1073/pnas.1200448109](https://doi.org/10.1073/pnas.1200448109)
- [56] Ferreira JV, da Rosa Soares A, Ramalho J, et al. LAMP2A regulates the loading of proteins into exosomes. *Sci Adv*. 2022 Mar 25;8(12):eabm1140. doi: [10.1126/sciadv.abm1140](https://doi.org/10.1126/sciadv.abm1140)
- [57] Mizushima N, Noda T, Yoshimori T, et al. A protein conjugation system essential for autophagy. *Nature*. 1998 Sep 24;395(6700):395–398. doi: [10.1038/265506](https://doi.org/10.1038/265506)
- [58] Otomo C, Metlagel Z, Takaesu G, et al. Structure of the human ATG12~ATG5 conjugate required for LC3 lipidation in autophagy. *Nat Struct Mol Biol*. 2013 Jan;20(1):59–66. doi: [10.1038/nsmb.2431](https://doi.org/10.1038/nsmb.2431)
- [59] Fader CM, Colombo MI. Autophagy and multivesicular bodies: two closely related partners. *Cell Death Differ*. 2009 Jan;16(1):70–78. doi: [10.1038/cdd.2008.168](https://doi.org/10.1038/cdd.2008.168)
- [60] Mauthe M, Orhon I, Rocchi C, et al. Chloroquine inhibits autophagic flux by decreasing autophagosome-lysosome fusion. *Autophagy*. 2018;14(8):1435–1455. doi: [10.1080/15548627.2018.1474314](https://doi.org/10.1080/15548627.2018.1474314)
- [61] Trajkovic K, Hsu C, Chiantia S, et al. Ceramide triggers budding of exosome vesicles into multivesicular endosomes. *Science*. 2008 Feb 29;319(5867):1244–1247. doi: [10.1126/science.1153124](https://doi.org/10.1126/science.1153124)
- [62] Ostrowski M, Carmo NB, Krumeich S, et al. Rab27a and Rab27b control different steps of the exosome secretion pathway. *Nat Cell Biol*. 2010 Jan;12(1):19–30; sup pp 1–13. doi: [10.1038/ncb2000](https://doi.org/10.1038/ncb2000)
- [63] Todeschini AL, Georges A, Veitia RA. Transcription factors: specific DNA binding and specific gene regulation. *Trends Genet*. 2014 Jun;30(6):211–219. doi: [10.1016/j.tig.2014.04.002](https://doi.org/10.1016/j.tig.2014.04.002)
- [64] Miller KN, Victorelli SG, Salmonowicz H, et al. Cytoplasmic DNA: sources, sensing, and role in aging and disease. *Cell*. 2021 Oct 28;184(22):5506–5526. doi: [10.1016/j.cell.2021.09.034](https://doi.org/10.1016/j.cell.2021.09.034)
- [65] Claeys Bouuaert C, Pu S, Wang J, et al. DNA-driven condensation assembles the meiotic DNA break machinery. *Nature*. 2021 Apr;592(7852):144–149. doi: [10.1038/s41586-021-03374-w](https://doi.org/10.1038/s41586-021-03374-w)

- [66] Desta IT, Porter KA, Xia B, et al. Performance and its limits in rigid body protein-protein docking. *Structure*. 2020 Sep 1;28(9):1071–1081 e3. doi: [10.1016/j.str.2020.06.006](https://doi.org/10.1016/j.str.2020.06.006)
- [67] Nivon LG, Moretti R, Baker D, et al. A Pareto-optimal refinement method for protein design scaffolds. *PLoS One*. 2013;8(4):e59004. doi: [10.1371/journal.pone.0059004](https://doi.org/10.1371/journal.pone.0059004)
- [68] Liu Y, Long YH, Wang SQ, et al. JMJD6 regulates histone H2A.X phosphorylation and promotes autophagy in triple-negative breast cancer cells via a novel tyrosine kinase activity. *Oncogene*. 2019 Feb;38(7):980–997. doi: [10.1038/s41388-018-0466-y](https://doi.org/10.1038/s41388-018-0466-y)
- [69] Niu K, Xiang L, Jin Y, et al. Identification of LARK as a novel and conserved G-quadruplex binding protein in invertebrates and vertebrates. *Nucleic Acids Res*. 2019 Aug 22;47(14):7306–7320. doi: [10.1093/nar/gkz484](https://doi.org/10.1093/nar/gkz484)
- [70] Yang L, Liu Q, Zhang X, et al. DNA of neutrophil extracellular traps promotes cancer metastasis via CCDC25. *Nature*. 2020 Jul;583(7814):133–138. doi: [10.1038/s41586-020-2394-6](https://doi.org/10.1038/s41586-020-2394-6)
- [71] Zhang Z, Bu H, Yu J, et al. The cell-penetrating FOXM1 N-terminus (M1-138) demonstrates potent inhibitory effects on cancer cells by targeting FOXM1 and FOXM1-interacting factor SMAD3. *Theranostics*. 2019;9(10):2882–2896. doi: [10.7150/thno.32693](https://doi.org/10.7150/thno.32693)
- [72] Kharchenko PV, Tolstorukov MY, Park PJ. Design and analysis of ChIP-seq experiments for DNA-binding proteins. *Nat Biotechnol*. 2008 Dec;26(12):1351–1359. doi: [10.1038/nbt.1508](https://doi.org/10.1038/nbt.1508)
- [73] Chen S, Zhou Y, Chen Y, et al. Fastp: an ultra-fast all-in-one FASTQ preprocessor. *Bioinformatics*. 2018 Sep 1;34(17):i884–i890. doi: [10.1093/bioinformatics/bty560](https://doi.org/10.1093/bioinformatics/bty560)
- [74] Li H. Aligning sequence reads, clone sequences and assembly contigs with BWA-MEM. *arXiv*. 2013;1303.3997. doi: [10.48550/arXiv.1303.3997](https://doi.org/10.48550/arXiv.1303.3997)
- [75] Zhang Y, Liu T, Meyer CA, et al. Model-based analysis of ChIP-Seq (MACS). *Genome Biol*. 2008;9(9):R137. doi: [10.1186/gb-2008-9-9-r137](https://doi.org/10.1186/gb-2008-9-9-r137)
- [76] Yu G, Wang LG, He QY. ChIPseeker: an R/Bioconductor package for ChIP peak annotation, comparison and visualization. *Bioinformatics*. 2015 Jul 15;31(14):2382–2383. doi: [10.1093/bioinformatics/btv145](https://doi.org/10.1093/bioinformatics/btv145)
- [77] Robinson JT, Thorvaldsdottir H, Winckler W, et al. Integrative genomics viewer. *Nat Biotechnol*. 2011 Jan;29(1):24–26. doi: [10.1038/nbt.1754](https://doi.org/10.1038/nbt.1754)
- [78] Tsuchiya KD. Fluorescence in situ hybridization. *Clin Lab Med*. 2011 Dec;31(4):525–42. doi: [10.1016/j.cll.2011.08.011](https://doi.org/10.1016/j.cll.2011.08.011)